



# CHALMERS

---



## **Solar Powered Bike Sharing System with Electric Bikes**

An overview of the energy system and the  
technical system design

Master thesis within the Master's Programme Industrial Ecology  
*Examensarbete inom civilingenjörsprogrammet elektroteknik*

FABIAN FOGELBERG

---

Department of Energy and Environment  
Division of Environmental System Analysis  
CHALMERS UNIVERSITY OF TECHNOLOGY  
Göteborg, Sweden 2014  
Report no. 2014:4



REPORT NO. 2014:4

# Solar Powered Bike Sharing System with Electric Bikes

An overview of the energy system and the technical system design

FABIAN FOGELBERG

Department of Energy and Environment  
*Division of Environmental System Analysis*  
CHALMERS UNIVERSITY OF TECHNOLOGY  
Göteborg, Sweden 2014

Solar Powered Bike Sharing System with Electric Bikes  
An overview of the energy system and the technical system design  
FABIAN FOGELBERG

In collaboration with Viktoria Swedish ICT

Tutors: Magnus Karlström and Magda Collado  
Examiner: Björn Sandén

© FABIAN FOGELBERG, 2014.

Report no. 2014:4  
Department of Energy and Environment  
*Division of Environmental System Analysis*  
Chalmers University of Technology  
SE-412 96 Göteborg  
Sweden  
Telephone + 46 (0)31-772 1000

Cover:

Concept image of a solar powered bike pool with electric bikes. © Fabian Fogelberg, 2014.

Chalmers Reproservice  
Göteborg, Sweden 2014

## Abstract

Combining Electric Bikes (E-bikes) with bicycle sharing systems could have a number of benefits. E-bikes reduce the human force needed for propulsion which facilitates longer and hillier rides relative regular bikes. The system could thus have more widespread network of stations, not only reaching more people but also enable commuting longer distances. It could also reduce the need for redistribution as users of regular bike sharing systems tend to only ride downhill.

The focus of this report has been to perform energy calculations and system design on solar powered E-bike pools. The geographical focus has been on Gothenburg, Sweden but the results can be applied to locations with similar latitude. The calculation methodology may however be applied to any other city around the world. It was shown that placing 0.2-0.8 m<sup>2</sup> solar panels per E-bike on the station's roof could supply enough energy to make the E-bike self-sufficient on a yearly basis despite high degree of system use. By increasing the solar panel area it was shown that there can be a net electric energy production on a yearly basis. At the maximum assumed solar panel area (about 3-3.8 m<sup>2</sup>/E-bike) there could be 600-800 kWh of solar energy fed to the grid per E-bike and year depending on the usage level.

Using a system that is on-grid and coupled with a stationary battery is seen as the best system design. That would enable origin marking of electricity and decrease the problem of intermittency with solar power. Reducing the interchange with the grid would also increase the system efficiency as the current do not need to be converted to or from AC as often.

*Keywords: electric bike, electric bicycle, solar power, e-bike, pedelec, BSS, shared bicycles, bike pool, bike sharing system.*

## Acknowledgements

This thesis would not have been if it were not for Stefan Pettersson at Viktoria Swedish ICT who found me this interesting project, thank you for that. Thank you Magda Collado at Viktoria Swedish ICT for your help along the way and for letting me take part in the E-bike project. Thank you Magnus Karlström at Chalmers Industriteknik for being my tutor, have met me for interesting discussions regarding the project and helped me with my text. Thank you Björn Sandén for being my examiner, taking your time for the interesting discussions we had along the way and for giving me feedback on the report. Thanks to the solar irradiation data provider SoDa for your data. Without it, I would not have been able to study the solar energy in such detail. A special thanks to Claire Thomas at SoDa for your help with the data access and for sorting out my confusions regarding the data. Thank you Johan Wedlin at Viktoria Swedish ICT for your proof-reading. Thanks to the all staff at Viktoria Swedish ICT who have welcomed me into your inspiring world and to my mum and dad, Karin and Hans Fogelberg, who gave me valuable comments on my report.

Now I want an E-bike.

# Abbreviations

AC	Alternating Current [A]
BLDC	Brushless DC motor
BHI	Beam (direct) Horizontal Irradiance [ $\text{W}/\text{m}^2$ ]
BSS	Bike Sharing System
BTI	Beam (direct) Tilted Irradiance
DC	Direct Current [A]
DHI	Diffuse Horizontal Irradiance [ $\text{W}/\text{m}^2$ ]
DTI	Diffuse Tilted Irradiance [ $\text{W}/\text{m}^2$ ]
E-bike	Electric Bike (pedal assisted)
E-BSS	Electric Bike Sharing System
GHG	Green House Gas
GHI	Global Horizontal Irradiance [ $\text{W}/\text{m}^2$ ]
GTI	Global Tilted Irradiance [ $\text{W}/\text{m}^2$ ]
$I_{sc}$	Short Circuit Current [A]
Li-ion	Lithium ion
mc-Si	Multi-crystalline silicon
MPP	Maximum Power Point
MPPT	Maximum Power Point Tracker
NiMH	Nickel Metal Hydride
NOCT	Nominal Operating Cell Temperature [ $^{\circ}\text{C}$ ]
PM	Permanent Magnets
PV	Photovoltaic
RTI	Reflected Tilted Irradiance [ $\text{W}/\text{m}^2$ ]
sc-Si	Single-crystalline silicon
STC	Standard Test Conditions
TC	Temperature Coefficient [ $\%/^{\circ}\text{C}$ ]
$V_{oc}$	Open Circuit Voltage [V]

# Contents

- 1. Introduction..... 1
- 2. Purpose & research questions ..... 3
- 3. Research methodology ..... 4
  - 3.1 Availability of solar power ..... 4
  - 3.2 Energy requirements of E-bikes ..... 5
  - 3.3 System design of charging stations ..... 5
- 4. Background ..... 6
  - 4.1 Solar energy ..... 6
    - 4.1.1 Variability of solar irradiance and irradiation ..... 8
    - 4.1.2 Solar Photovoltaic and energy calculations..... 8
    - 4.1.3 Solar cell characteristics ..... 10
    - 4.1.4 Mounting and tracking technology ..... 12
  - 4.2 Electric bikes ..... 13
    - 4.2.1 E-bike batteries..... 15
    - 4.2.2 Electric motor and motor control ..... 16
    - 4.2.3 Human power input..... 17
  - 4.3 Bike sharing systems ..... 17
    - 4.3.1 Taking the leap from BSS to E-BSS ..... 20
- 5. Methodology for calculations on a solar powered E-bike sharing pool ..... 21
  - 5.1 Solar energy calculations ..... 21
    - 5.1.1 Irradiance data ..... 21
    - 5.1.2 Case study on four possible station locations in Gothenburg ..... 22
    - 5.1.3 Losses in the solar cell ..... 23
    - 5.1.4 Shading in the urban environment ..... 24
    - 5.1.5 Specifications on the solar panel installation ..... 26
  - 5.2 Modelling an E-bike ..... 26
    - 5.2.1 Power during acceleration and deceleration..... 27
    - 5.2.2 Power to overcome air drag..... 27
    - 5.2.3 Power to overcome rolling resistance ..... 28
    - 5.2.4 Power during climbing ..... 28

5.2.5	Regenerative braking.....	29
5.3	Modelling an E-BSS system.....	30
6.	Results.....	34
6.1	Available solar energy and weather.....	34
6.2	E-bike electric energy use.....	37
6.3	E-BSS energy results .....	38
7.	Discussion .....	43
7.1	Weaknesses and uncertainties .....	43
7.2	The energy system .....	44
7.3	The operational perspective.....	45
8.	Conclusions.....	47
9.	References.....	48
	Appendix 1 .....	52
	Appendix 2 .....	54
	Appendix 3 .....	58
	Appendix 4 .....	62
	Appendix 5 .....	66
	Appendix 6.....	68
	Appendix 7 .....	69



# 1. Introduction

Climate change from increased concentration of carbon dioxide in the atmosphere was acknowledged already back in the year 1896 (Arrhenius, 1896). It is however not until recent decades that discussions have emerged, and plans been developed, on how our emissions of Green House Gasses (GHG) should be reduced. The transport sector accounted for 13% of the global GHG emissions in 2004 (IPCC, 2007, p. 29). In addition to the global challenge of GHG emissions, many cities around the world face problems with local air pollution and congestion. Decreasing air pollution on a local — and a global — level can be accomplished by switching to vehicles with fuels that have lower environmental impact than fossil fuels; such as electric vehicles or bio-fuels. However, this does not directly affect congestion.

Around a third of the trips made by car in Europe are shorter than 3 km, and half of the trips shorter than 5 km (IPCC, 2007, p. 51). This means that there is a potential for efficiency and air-quality improvement by switching to more energy efficient and less polluting modes of transport that can replace these short distance trips. One alternative is to increase bicycling which could reduce the need for taking car or public transport short distances as well as reduce congestion. One of the methods to increase bicycling in cities is to set up Bike Sharing Systems (BSS) that can be accessed by locals or tourists for a fee. There are currently more than 600 cities with BSS globally (ITDP, 2013, p. 10). The number of bikes in those systems exceeds 700 000 (ITDP, 2013, p. 13). By providing a large network of stations with shared bicycles, it is possible to supply an efficient, convenient and cheap mode of transport. These types of systems have been proven successful. In Barcelona, a maximum number of registered users per bike has been set, as well as prices increased in order to ensure an efficient system (OBIS, 2011, p. 59). One drawback with current BSS is that they are used for short rides in city centres and uphill rides have been seen to be avoided by users which increases the need for redistribution by truck (ITDP, 2013, p. 116). BSS uses commonly available trucks and cars on the market for their redistributions. They thus rely mostly on fossil fuels. Admittedly, the environmental impact from redistribution may be reduced if the car or the truck is powered by renewable power sources but reducing the need of redistribution also decreases the operating costs and congestion.

Recent developments on pedal assisted Electrical Bikes (E-bikes) and regulations surrounding them have led to a growing market of E-bikes all around the world. Especially in China where 9 out of every 10 E-bikes are sold (Navigant Research, 2014). E-bikes could potentially be one of the first type of electric vehicles to reach large-scale diffusion in Sweden (excluding trams and trains). Not only are they energy efficient, but also cheap relative other electrified transport modes. They enable rides in hilly and windy conditions where cyclists would reduce their speed significantly. Longer rides are also possible as the rider's effort is reduced. Thanks

to the characteristics of E-bikes they have a greater potential to replace car trips than regular bikes (Langford, et al., 2013). Introducing Bike Sharing

## Electric bike

A pedal assisted electric bike (E-bike or Pedelec) is a bike with an electric motor that only supplies electric power when the pedals are rotating. The motor must be turned off at 25 km/h and the maximum designed motor power is 250 W.

Systems with E-bikes (E-BSS) could open up their use to a broader audience. The potential for modal shift from fossil fuel powered transport modes would thus increase. Furthermore, a roof may be placed on top of the E-bike station that could serve as combined weather protection and provider of electric energy by installing solar panels on the roof. If the available solar energy is sufficient, it could for example keep the system off-grid which means that stations can be placed temporarily where needed, e.g. close to festival areas or sports events. Placing solar panels on station roofs would introduce solar energy in places that otherwise would not have been considered. An E-bike charged with electricity from the sun may be one of the most efficient means of transport there is (see Appendix 1). The main reason is because its mass is lower than a car's or a scooter's and thus less energy is required for propulsion. The second reason is that bio-fuels or regular cycling requires conversion of solar energy to chemical energy which is characterised by low energy conversion efficiencies relative a solar panel.

There are several E-bike pools around the world. Some have been running for a few years and some are recently started. To name a few there are: GoBike in Copenhagen, EnelooP SANYO in Tokyo, CycleUshare in Knoxville and E-call a Bike in Stuttgart. Of those systems, two are coupled with solar panels, EnelooP SANYO and CycleUshare. As CycleUshare is built and operated by the University of Tennessee-Knoxville, research is being made and published on E-BSS (University of Tennessee-Knoxville, 2014). However, many questions are still to be answered as the use of E-BSS is far from large-scale in comparison to regular BSS. Also, little information has been found on the synergy between solar panels and E-BSS. This is thus the focus of this report in which the energy balance between the solar energy and E-bike energy use is studied in detail for different system designs.

## 2. Purpose & research questions

This master's thesis is part of a pre-study at the research institute Viktoria Swedish ICT that aims at evaluating how E-BSS can be used as an urban mobility transport mode and determine its implementation feasibility in the Western Sweden Region. The main objective of this thesis is to investigate the energy system of E-BSS with solar panels on the stations' roofs. The geographical focus is within the Western Sweden Region and more specifically, the city of Gothenburg. The reason for the narrow geographic boundary is that solar irradiation varies with location. Numeric results from the thesis may however be applied to nearby cities and other locations at similar latitude as long as there are no major differences in irradiation. The methodology presented in this report is however be applicable to other cities around the world who want to learn more about how to develop and implement an E-BSS equipped with solar panels.

A large share of the investigation is performed on a per E-bike basis as the numbers of E-bikes in a station can vary. The study is divided into three parts: A study on the available energy from the solar panels in urban environment, the energy use of E-bikes and the resulting energy balance depending on system design. The research questions to be answered within each part are:

1. Solar energy:
  - What is the availability of solar energy in urban environments?
2. E-bikes:
  - What is the electric energy use of an E-bike?
  - What is the typical usage of bikes in a pool system?
3. System evaluation:
  - How much installed solar power is required per E-bike on a yearly basis in Gothenburg, Sweden?
  - How does the solar panel area affect the yearly energy balance of the system?
  - What type of system design is most suitable, on- or off-grid? With or without a stationary buffer battery?
  - What effect do the system design options have on the energy balance?
  - How should battery depletions be avoided?
  - What are important to think about when setting up an E-BSS?

### 3. Research methodology

This study is mainly focused on calculations of the energy balance of solar powered E-bike pools. The first step is to perform a literature review on solar energy, E-bikes and BSS. The purpose of this review is to get knowledge on how each component work, their energy use/generation and how they would interact in a pool system. The literature is as far as possible collected from scientific databases such as Chalmers library's database search tool Summon. Peer reviewed research papers were prioritised but other information types such as books or reports can be collected from there as well. In cases where the scientific literature does not have the information needed, such as specifications on commercial products, web searches was performed to find information from other sources.

The study is divided into three main parts:

1. Calculations of available electrical energy from the solar panels.
2. Calculations of energy required of the E-bikes.
3. Evaluation on system design by literature review of current BSS and BSS data and results from the two first parts.

The software Matlab from Mathworks is used as the main tool in all calculations of the E-bike's energy use and the availability of solar energy.

#### 3.1 Availability of solar power

To estimate the available electric energy from solar panels there are a number of parameters that need to be identified and estimated properly. The first step is to estimate the available solar irradiation. To do this, detailed datasets of solar irradiation data is needed. This information is collected from the solar irradiation data provider SoDa (SoDa, 2014). They provide irradiation data derived from satellite and ground measurements (ibid.). The datasets used consists of hourly irradiation towards Gothenburg from February 1, 2004 to December 31, 2005. If data are missing or corrupted, interpolation is considered to enable calculations over the entire period.

In ideal cases, all solar energy available would be collected by the solar panels but in a city environment this is not always the case since buildings will shadow the irradiation. A method of estimating these losses was developed. When the sunlight hits the solar panels, a number of different losses will occur during the conversion to electric power. These will be dependent on a number of factors such as type of solar cell technology used, outdoor temperature etc. Some parameters can be determined by literature review of solar cell research while others depend on system design and specific choice of system components.

### **3.2 Energy requirements of E-bikes**

There are numerous different things that will affect the energy use of the E-bikes. The energy requirements will vary heavily depending on the choice of route, the rider's weight, the E-bike's specifications, etc. A few of these parameters were identified in the literature review but some are dependent on actual system design. To get further insight on how BSS are being used, data from running BSS was collected and analysed.

### **3.3 System design of charging stations**

By combining the simulation results of available energy from the solar panels with the energy requirements of the E-bikes it is possible to study different options of system design. Independent of the amount of data collected, there is some things that cannot be determined with great certainty as this report is of exploratory nature. This means that some results might not apply to a real system. To deal with this problem, it was tried throughout the report to analyse the system carefully to ensure that the drawn conclusions in the end will be relevant for a real case despite changes in for example use of the system.

## 4. Background

This chapter presents background information on solar energy, E-bikes and BSS. Section 4.1 starts by introducing solar radiation to explain the variability of solar energy and the energy levels involved. The section is ended with an introduction to solar cell technologies and the factors affecting the electric power output. Section 4.2 includes information on E-bikes from legal and technical perspectives including specific descriptions of components. Finally, section 4.3, includes information and data on bicycle sharing schemes currently in place.

### 4.1 Solar energy

Everyone knows the power of the sun. If you are out in direct sunlight you feel your skin warming up and anyone who has ever set foot into a car parked in direct sunlight knows the sauna-like heat that hits you when opening the door. The solar irradiance perpendicular towards the top of earth's atmosphere — also known as the solar constant — is roughly  $1360 \text{ W/m}^2$  (Kopp & Lean, 2011). This is the sum of all incoming electromagnetic radiation. The share of the solar constant that reaches the ground depends on many factors. The atmosphere will reflect, absorb and scatter the irradiance based on its chemical composition such as water vapour content, cloud coverage and amount of aerosols (Weier & Cahalan, 2003). Another factor is the inclination of incoming light; the lower the angle, the lower the irradiance towards a surface. This is one of the reasons behind the relationship of decreased incoming light towards the ground with increased distance from the equator. A lower angle of the sun relative to the ground also means that the light travels through a larger air-mass and thus the light intensity decreases due to previous mentioned factors.

The measure of the radiation's total power is noted irradiance and can be expressed in  $\text{W/m}^2$ . By integrating the irradiance you get the energy, or irradiation, that can be expressed in for example Wh or kWh per  $\text{m}^2$ . It is important to note that the surface may be either horizontal, or inclined in a certain angle relative the incoming irradiance. This angle will affect the amount of irradiance falling onto the surface. To be able to analyse the irradiance in further detail, it can be split up in three main components: Direct, reflected and diffuse irradiance.

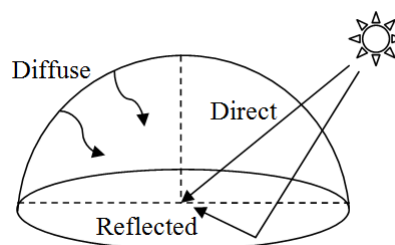


*Figure 1. Direct irradiance originates straight from the sun, reflected irradiance from reflections in the ground (thus hits tilted planes only) and diffuse irradiance originates from the entire hemisphere.*

Figure 1 shows how the three main irradiance components are defined. The direct irradiance is the irradiance that comes straight from the sun disk, the reflected irradiance originates from

reflections in ground and the diffuse component represents irradiance coming from the entire hemisphere (excluding the sun disk) due to scattering and reflections in the earth's atmosphere and clouds. The reflected irradiance originates from ground; it is thus zero when evaluating the irradiance towards a horizontal plane. The reason for why the irradiance is split up in different components is that they behave differently and the split thus enable a more detailed analysis.

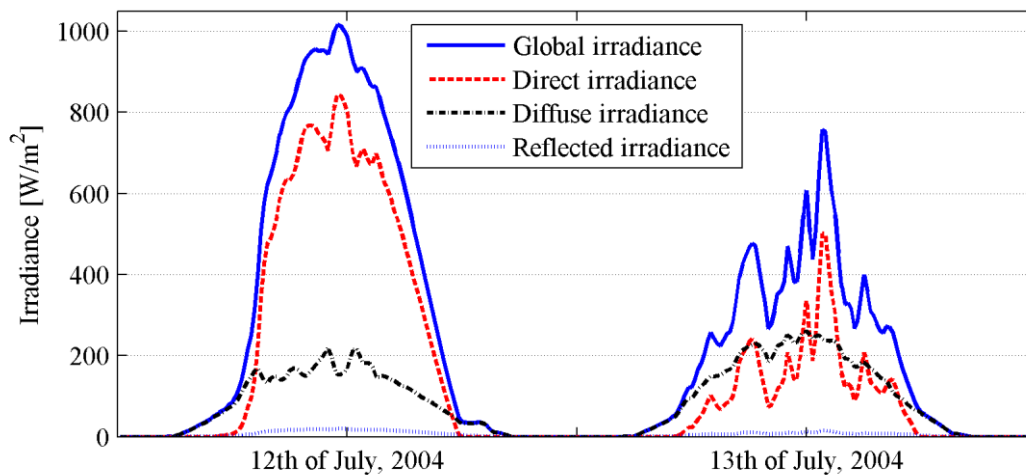


Figure 2. Example of solar irradiance in Gothenburg, Sweden, during two days in July, 2004. The global irradiance is the sum of all irradiance components (solid). The direct irradiance is dashed (red), the diffuse dashed-dotted (black) and the reflected dotted (blue). All components are towards a shadow-free surface tilted  $40^\circ$  ( $0^\circ$  being horizontal) and south-facing. Data: SoDa (2014).

The sum of the direct, the reflected and the diffuse irradiance is called the global irradiance, which is what is shown as a solid line in Figure 2. The maximum irradiance seen in Figure 2 — just above  $1000 \text{ W/m}^2$  — represents typical maximum irradiance perpendicular to the sun at ground level (IEA, 2011). The first day in Figure 2 shows smooth global irradiance with the direct irradiance being the dominant component; this means a clear and sunny day. On the second day, the irradiance is much lower due to clouds shading the surface. The diffuse component has therefore a larger share of the global irradiance. It can also be noted that the reflected irradiance (dotted in Figure 2) is small during both days. In order to keep the different irradiance components apart it is useful to introduce abbreviations as seen in Table 1.

**Table 1. Abbreviations for the different irradiance components.**

Abbreviation	Irradiance component
GHI	Global Horizontal Irradiance
BHI	Beam (direct) Horizontal Irradiance
DHI	Diffuse Horizontal Irradiance
GTI	Global Tilted Irradiance
BTI	Beam (direct) Tilted Irradiance
DTI	Diffuse Tilted Irradiance
RTI	Reflected Tilted Irradiance

### 4.1.1 Variability of solar irradiance and irradiation

There are great variations in solar irradiance and irradiation that must be acknowledged and understood in order to analyse solar powered systems properly. In one second the irradiance may fall from  $1000 \text{ W/m}^2$  to a tenth, if a thick cloud suddenly shades the sun. On a day-to-day basis, as exemplified in Figure 2, the irradiation was  $7.8 \text{ kWh/m}^2$  the first day to drop to  $4.3 \text{ kWh/m}^2$  the next due to different weather.

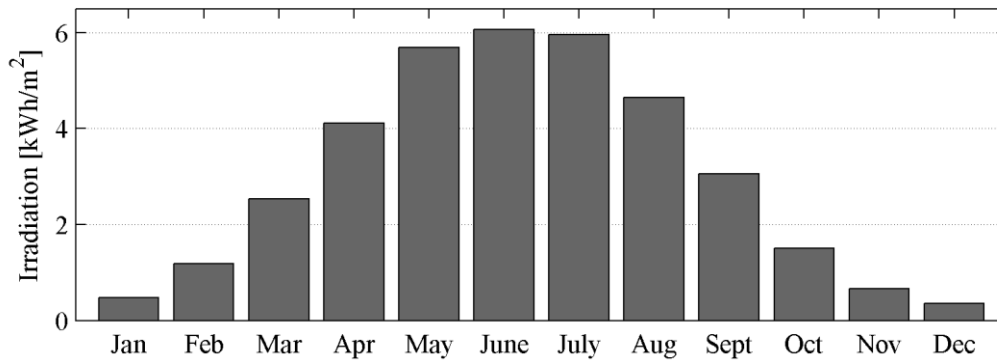


Figure 3. Average daily Global Horizontal Irradiation (GHI) for each month in Gothenburg, Sweden, towards a horizontal and shadow-free surface. Data is averaged from 1983 to 2005. Data: NASA (2014).

Not only weather affects the irradiation, but also the inclination towards the sun. Figure 3 shows the average daily irradiation towards a horizontal surface for each month in Gothenburg, Sweden. As the city is located at high latitude ( $58^\circ$ ), the sun's inclination is low during winters and increasing during summers. The irradiation thus follows a similar pattern. Differences in weather patterns may also cause the long-term average irradiation to vary with up to  $\pm 30\%$  on a monthly scale and  $\pm 10\%$  on a yearly (NREL, 2011). An implication of the intermittency of the solar energy is that some sort of buffering is necessary if the load does not match the irradiation perfectly.

### 4.1.2 Solar Photovoltaic and energy calculations

The first silicon Photovoltaic (PV) cell was developed by Bell Labs in the U.S. during the 1950s (United States Department of Energy, 2010). The cell had a conversion efficiency of solar to electric power of 4% which is a record that continuously has been broken ever since. The highest efficiency as of today is 44.7%, measured in lab environment (Dimroth, 2013). Commercial solar panels however have lower efficiencies as shown in Table 2 (IEA, 2011, pp. 114-115; Green, et al., 2013). At first, PVs were used in niche applications in for example space, rural electrification and telecommunication (IEA, 2011, p. 47). Later developments in production and efficiency, as well as governmental market support programmes, have led to a PV market that is expanding each year with prices that decreases continuously on long-term scale (ibid.).

**Table 2. Typical efficiency of commercial solar panels.**

<b>Solar cell technology</b>	<b>Typical range of commercial panel efficiency (%)</b>
Single-crystalline Silicon (sc-Si)	14-22
Multi-crystalline Silicon (mc-Si)	12-19
Thin films	4-19

There are a number of solar cell technologies on the market but 85% of the market is dominated by the crystalline silicon technologies (IEA, 2011). Within that category there are two main technologies: Single-crystalline (sc-Si) and multi-crystalline (mc-Si) solar cells. Sc-Si solar cells are made from silicon wafers with very high purity which results in higher efficiency than mc-Si (see Table 2). The second largest market share is thin film solar cells. Thin films is the name for solar cells that are produced by applying each layer one at a time onto a substrate such as glass or a flexible surface (Poortmans & Arkhipov, 2006, p. xix). One widespread thin film technology is the Amorphous Silicon (a-Si) solar cells — the type used in calculators — which often are cheaper to produce than crystalline silicon solar cells. However, their efficiency is lower. Another type of thin film is multi-junction silicon solar cells. They use different layers of solar cells to be able to convert a broader spectrum of the incoming irradiance into electricity (IEA, 2011). The efficiency of multi-junction solar cell differs with the layers used but it may reach up to 19% on commercial panels (Panasonic, 2014).

In any installation it is important to know the estimated lifespan in order to calculate long-term feasibility. Common market praxis in the PV industry is to guarantee that the solar panel will generate at least 80% of the rated output power after 25 years (IEA, 2011, p. 114). The system cost for a small (0-20 kW) grid-connected solar panel system in Sweden was around 15 SEK/W in 2013 (Energimyndigheten, 2014). The cost figure is for the most common cell technology, i.e. either sc-Si or mc-Si.

### 4.1.3 Solar cell characteristics

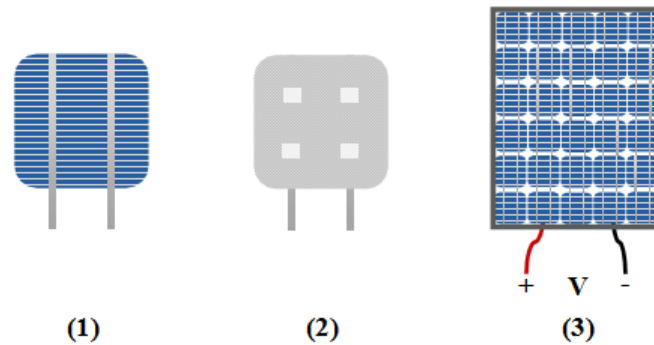


Figure 4. Example of mc-Si or sc-Si cell and panel. (1) Front of solar cell: Horizontal stripes collect the current and minimises the resistance and are connected to bus bars (vertical), used for connection to other cells. (2) Back of cell: Square contact points are used to connect bus bars from previous cell. (3) Panel layout: All cells connected in series. Source: Own work.

A typical crystalline silicon solar cell is shown in Figure 4, (1). The horizontal lines on the front help to minimise the resistance and thus increase the efficiency and the vertical lines are used to connect cell to back of the next one (Figure 4 (2)). A crystalline silicon solar cell has an open voltage ( $V_{oc}$ ) of about 0.5-0.6 V when fully irradiated and generates short-circuit current ( $I_{sc}$ ) proportional to the incoming irradiance (Rauschenbach, 1980, pp. 55, 198). To get a useful voltage in a PV system, several cells are thus connected in series and usually mounted in a rigid glass-framed panel as exemplified in Figure 4, (3). To further increase the voltage, several panels can be series connected and to increase the current, they can be parallel connected. In this way it is possible to configure the amount of series and parallel connections to get a desired voltage and current.

To prevent current to flow in the wrong direction, e.g. from a battery to a solar panel or from one panel to another in a parallel configuration, a blocking diode is usually added on each panel (Rauschenbach, 1980, p. 74). A diode works in such a way that when it is forward biased (typically about 0.7-1 V) it conducts and when a negative voltage is applied, it acts like a circuit breaker (ibid.). An example of operation is if an 18 V solar panel is connected to a 12 V battery. During the day, the voltage of the solar panel exceeds the voltage of the battery, and current will thus flow into the battery. On the night however, the solar panel's open voltage will be 0 V and current will thus flow from the battery to the solar panel instead, not only draining the battery but potentially also damaging the solar panel. By adding a diode between the panel and the battery, it is possible to prevent current to flow in the wrong direction night-time while still enabling battery charging daytime.

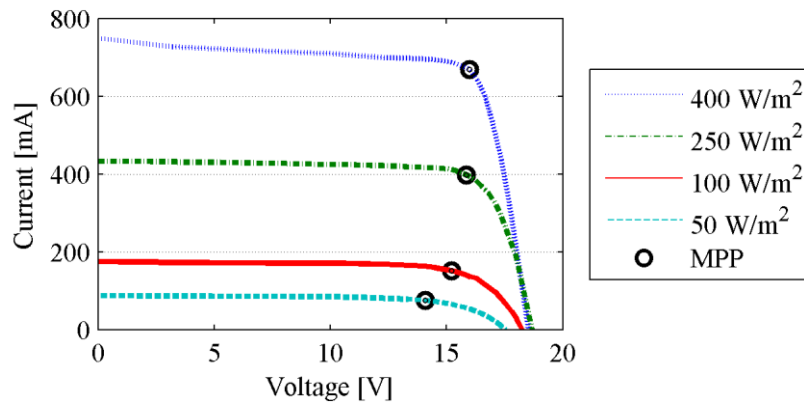


Figure 5. Typical characteristics of a silicon solar panel for different loads and irradiance levels. The circles mark maximum power points at each irradiance level. Data: Measurement on a mc-Si panel at Chalmers University of Technology, 2012.

An example of characteristic of a solar panel (or cell) is shown in Figure 5 for four different irradiance levels ranging from  $50 W/m^2$  to  $400 W/m^2$ . The curve was created by adjusting the load connected to a mc-Si solar panel and measuring the output current and voltage simultaneously. The power output in any point is given by voltage times current; this means that the maximum power output is obtained when the area beneath each curve is highest. This operating point is called the Maximum Power Point (MPP) and is marked with circles in Figure 5. As the load in a PV system may vary and the MPP is dependent on irradiance (as seen for the different lines in Figure 5), it is important to apply a tracking technology that ensures operation at MPP. This is performed by a Maximum Power Point Tracker (MPPT) which is the name for any power electronic device that is able to adjust the load to ensure operation at MPP for maximum energy yield. The linear relationship in short circuit current and incoming irradiance can be seen in Figure 5 by comparing the current at 0 V ( $I_{sc}$ ) for  $50 W/m^2$  and  $100 W/m^2$  where the current is approximately doubled. What also can be noted is that there is a decreasing relationship in open voltage (i.e. at 0 A) with decreasing irradiance. The MPPT is usually incorporated in the grid tie inverter that converts the Direct Current (DC) to Alternating Current (AC) fed to the electrical grid. It can also be incorporated in a battery charge controller designed to operate off-grid.

A common test procedure called Standard Test Conditions (STC) has been developed by the solar PV industry in order to have consistent information on solar panels. The test uses an artificial light source emitting a light spectrum called AM1. A spectrum which resembles the spectrum from the sunlight at sea level a clear day. The total irradiance of this light source is  $1000 W/m^2$  and the cell temperature of the tested solar cell or panel is held at  $25 ^\circ C$ . At these conditions, the output characteristics is measured similar to what is shown in Figure 5 and the MPP on that curve is the rated output power of the panel (Rauschenbach, 1980, p. 389). The rated power output from a solar panel is referred to as peak watts ( $W_p$ ) of installed power. Another test that usually is performed by solar panel manufacturers is the Nominal Operating Cell Temperature (NOCT). It is used to estimate the cell temperature under conditions that are

more common in field than the STC. Those specifications are: 800 W/m<sup>2</sup> irradiance, 20 °C ambient temperature and 1 m/s wind speed (Alonso García & Balenzategui, 2004).

The efficiency of a solar cell, or panel, is described by the ratio between the electrical output and the total incoming irradiance;

$$\eta = P_{el}/P_{solar}. \quad (1)$$

By solving for electrical power we get,

$$P_{el} = P_{solar}\eta = GA\eta, \quad (2)$$

where  $G$  is the total irradiance in W/m<sup>2</sup>,  $A$  the area in m<sup>2</sup> and  $\eta$  the conversion efficiency. A problem with the efficiency,  $\eta$ , is that it is dependent on temperature; the higher the temperature, the lower the efficiency (Rauschenbach, 1980, p. 74). This relationship will be further described in section 5.1.3.

#### 4.1.4 Mounting and tracking technology

To maximise the energy yield from fixed solar panels, they should generally be mounted towards the south<sup>1</sup>. In some cases however, e.g. when buildings are shading the panels it could be more beneficial to point the panels more east- or westwards. The tilt can be chosen to get the maximum yearly energy yield or optimised for another period depending on application. If for example an off-grid system should be designed that measures temperature and transmits the data to a weather institute, it is best to mount the panels so that the energy yield is highest during the period with lowest irradiation to ensure full-year operation (e.g. December as seen in Figure 6). The yearly optimal tilt angle will generally be higher the more North of the equator you are as the sun angle thus will be lower. If it is physically possible, the solar panels can be mounted on a tracking device that estimates where the irradiance is highest on the sky and turns the panels towards that point. There are a number of different tracking solutions on the market but two types can be identified: 1-axis and 2-axes tracking (either just azimuth or tilt, or both).

<sup>1</sup> In the Northern hemisphere; vice versa in the Southern hemisphere.

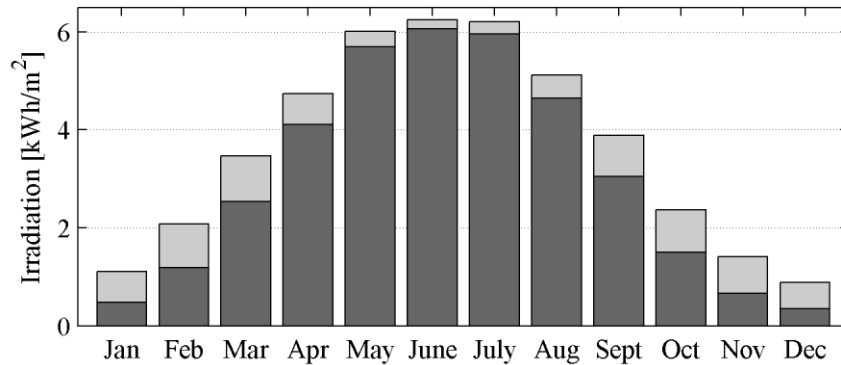


Figure 6. Average daily irradiation per month in Gothenburg, Sweden. Dark grey: Towards a horizontal surface. Light grey: Extra energy yield with 1-axis tracking (south-facing and changing tilt). Data: NASA (2014).

The energy gain from using tracking compared to fixed position will vary depending on location and how well the tracking performs. An example of the irradiation towards a horizontal surface and one with 1-axis tracking (changing tilt) is shown in Figure 6. The energy gain due to tracking during the winter months is more than the summer months due to the low solar angle wintertime. The yearly energy gain of the 1-axis tilting compared to the horizontal case in Figure 6 is 20%. A computer model for locations in Germany concluded that the yearly energy yield compared to fixed tilt could be increased with 10% for 1-axis tracking on an azimuth plane, 25% when changing the tilt instead and 29% when using a 2-axes tracking system (Breyer & Schmid, 2010).

## 4.2 Electric bikes

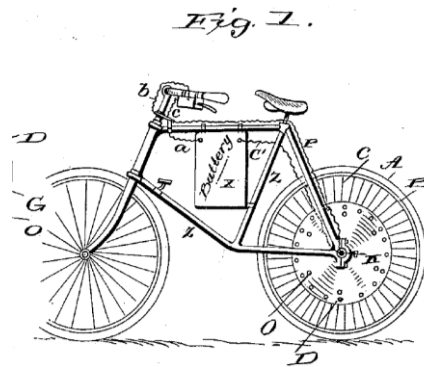


Figure 7. Electrical bike as figured in a patent from 1895. The motor is mounted on the rear wheel, the battery in the frame and the power switch on the handle. Note the lack of pedals. Drawing from a patent by Bolton Jr. (1895).

One of the first patents of electrical bikes was registered almost 120 years ago by Ogden Bolton Jr. (see Figure 7) (Bolton, 1895). The concept Bolton Jr. patented is similar to the E-bikes of today. An E-bike is — narrowed down to its basics — a regular bicycle equipped with an electrical motor, a battery and some electronics and switches that controls power levels. Since it is powered by two energy sources, pedalling and electricity, it can be classified

as a hybrid vehicle. For an E-bike to be legal in Sweden it has to fulfil a set of requirements according to the law (*Lag(2001:559) om vägtrafikdefinitioner*):

- Electrical motor may only be active while pedalling (unless speed is below 6 km/h).
- Maximum rated power of motor<sup>2</sup>: 250 W.
- No motor power may be provided at speeds above 25 km/h.

The EU directive 2002/24/EC also states that the power must be progressively reduce as the bike approaches 25 km/h, this is however not needed for E-bikes in Sweden. The fact that pedalling is not needed for speeds below 6 km/h can be especially practical when walking the bicycle uphill or cruising in walking speed. The requirements on E-bikes differs from country to country, but one that stands out is the U.S. who allows 750 W motor power and speeds up to 32 km/h without the need for pedalling (Morchin & Oman, 2006, p. 21).



*Figure 8. Example of typical commercial E-bike. The motor is in this case placed in the hub of the front wheel (rated at 250 W) and the battery and its electronics is enclosed in the black box right of the rear wheel. Typically, there is also a small control panel on the handles. Reproduced with permission of EcoRide (2014).*

An example of a commercially available E-bike is shown in Figure 8. The motor is usually placed in the front or rear wheel (called hub motor) but sometimes on the crank shaft (Atkinson, 2012) or mounted directly on the wheel (Rubbee, 2014). The location of the battery may vary depending on bike design but typically, the producers try to place it as low as possible for an optimum centre of gravity. There is usually also a control panel at the handle (not seen in Figure 8) that is used to turn on and off the E-bike function, set different power level options and monitor the battery level.

<sup>2</sup> Note: The rated power of the motor is the mechanical. The electrical power is thus higher due to losses in the motor and the rest of the electrical system. An electrical motor may also provide higher power than the rated during short periods of time.

### 4.2.1 E-bike batteries

A battery in an E-bike should have capacity large enough to keep the range at a level that meets the user's demand, but also meet technical requirements such as safety and be able to supply enough power to the motor. There are a number of different battery technologies on the market. A short review of twelve different E-bike producers<sup>3</sup> in Europe and USA revealed that all of them use Lithium Ion (Li-ion) batteries. Although this short investigation makes no claim to be complete, it is safe to say that Li-ion batteries are a common technology for western E-bike producers to use.

It was found that a common battery capacity is 10 Ah in a 36 V system. In energy that is equal to about 360 Wh assuming that the battery voltage does not change throughout the discharge cycle and that the State of Charge (SOC) may reach 0%. Li-ion batteries are in the upper range of energy density compared to other technologies (Morchin & Oman, 2006, p. 154) and they also last longer than other technologies (*ibid.*). The energy density of commercial Li-ion batteries is in the range of 100-250 Wh/kg (Panasonic, 2014) whereas the cheaper alternative, Lead Acid batteries, is around 30 Wh/kg (Morchin & Oman, 2006, p. 154). A drawback with Li-ion batteries is their high initial cost, however, when taking a lifecycle cost perspective they can still be cheaper than e.g. Lead Acid batteries (Morchin & Oman, 2006, p. 36). The cost of battery replacement for a Swedish E-bike user is about 3000 SEK (EcoRide, 2014; Lifebike, 2014).

The charge temperature of Li-ion batteries is about 0-45°C but it can discharge in the range of -20°C to 60°C (Cadex, 2014). No charging should be permitted if the battery temperature is below 0°C as this could damage the battery (*ibid.*). In the window of 0° to about 5°C, it is necessary to decrease the charge current (*ibid.*).

Another factor that is of importance for the choice of battery technology is the performance during heavy discharge. Such conditions can be riding steep uphill or in strong headwind. A Lead Acid battery will for example lose a large share (>50%) of its rated energy capacity during heavy continuous discharge compared to low discharge rates due to high internal loss (Zirnheld & Muffoletto, 2011). Nickel Metal Hydride (NiMH) and Li-ion batteries on the other hand lose less than 10% during similar conditions (*ibid.*). Charging the battery requires a charger that monitors the battery properly in order to avoid battery cell failure (Morchin & Oman, 2006, p. 92). Li-ion batteries could for example explode or catch fire if over-charged (*ibid.*).

<sup>3</sup> Investigated E-bike producers: EcoRide, Batbike, Sjösalä, Crescent, Lifebike, BionX, Easy Motion USA, Apollo, Monark, e-Victoria, MyEco and Kalkhoff.

### 4.2.2 Electric motor and motor control

An electrical motor is usually composed of a stator and within it a rotor. The design of the rotor and stator varies depending on motor technology. What all have in common is that a varying magnetic field within the machine is needed for continuous rotation. One type of motor that has been used since the early days of E-bikes is the brushed Direct Current (DC) motor (Bolton, 1895). In that machine, the rotating magnetic field is created by pole-switching every half turns by means of a brush between the stator and the rotor (Morchin & Oman, 2006, p. 112). However, this design has some drawbacks; the brush will eventually wear out and the efficiency is low due to resistive losses from the brush (*ibid.*).

Today, there are many different types of motors on the market but the one commonly used in E-bikes is Brushless DC motors (BLDC) (Muetze & Tan, 2007). The efficiency of BLDC is higher than the brushed variant thanks to the lack of a brush and that Permanent Magnets (PM) is used for magnetisation instead of current through coils (Muetze & Tan, 2007; Morchin & Oman, 2006, p. 115). A drawback with the BLDC motor is that needs more advanced motor control than the brushed motor type (Sandqvist, 2014). The short overview of the twelve E-bike producers mentioned in section 4.2.1 also showed that ten producers stated the motor technology used and nine out of them were BLDC motors.

The motors may be equipped with internal gears, or not, depending on design. Gears are used to reduce the motor speed from motor to wheel. Geared BLDC motors are commonly used on cheaper E-bikes as high efficiency is easier — and cheaper — to obtain with high motor speeds (Morchin & Oman, 2006). More expensive E-bikes may use gearless BLDC motors that are more expensive to build and control. The benefit of gearless drive is lower noise and no wear on internal gears. The efficiency of BLDC motors for E-bike applications is typically around 80% (Starschich & Muetze, 2007; Morchin & Oman, 2006, p. 33). A new motor type that has shown efficiency up to 90% in E-bikes is the transverse flux machine (Pompermaier, et al., 2012). This is however a new type of motor that not only costs more to produce but also requires even more complex control than the BLDC machine (*ibid.*) which makes the system more expensive (MyEco, 2014).

How the motor is controlled varies with manufacturers. Typically, the E-bike producers incorporate a control panel from which the user can turn on or off the electrical assist and set the power level of the motor. On cheaper E-bikes, a cadence sensor is used to identify if the pedals are spinning or not (Electricbike.com, 2013). If they are, the motor is turned on with a constant power level set by the user or controlled by a manual throttle (*ibid.*). This control strategy means that the E-bike can go without any force provided by the rider as long as the pedals are spinning. On more expensive E-bikes, a torque sensor is used to add electrical power proportional to what the rider puts in (*ibid.*). This results in lower total energy consumption and a more intuitive handling than using a cadence sensor (*ibid.*). The manufacturer Bosch for example, uses torque sensors in their E-bike drivelines (Bosch, 2014).

Their ratios of electric power to human can be set from 0.3:1 to 2.75:1 with a 1:1 ratio being the normal setting (ibid.). A 1:1 ratio means that the electric motor will provide equal amount of power as the rider. A third control strategy used is that the motor controller tries to reach a speed reference set by the user (EcoRide, 2014). The electric efficiency of the control system is unknown for most commercial E-bikes but one team that built an E-bike for research purposes reported efficiency above 94% (Spagnol, et al., 2012).

### 4.2.3 Human power input

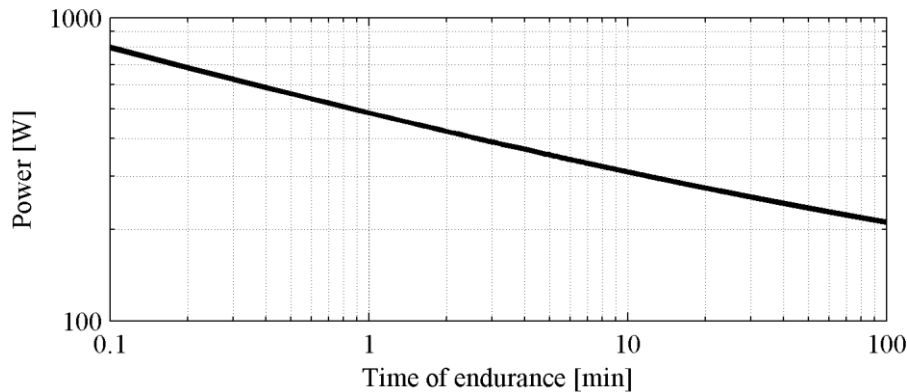


Figure 9. Example of the human endurance and power output while pedalling. Equation used from Morchin and Oman (2006).

The power provided by the rider is highly individual. An example of human power output during heavy pedalling is shown in Figure 9. More than 500 W may be supplied by a well-trained cyclist during short periods of time (<1 s). To put it in relation; one horsepower is 736 W which is the power needed to lift 75 kg, one meter in one second. For longer periods of time however, the maximum mechanical power is around 200-300 W. These figures obviously vary with factors such as age, sex and physical condition. An example of average human power output during a city ride on a bicycle without electrical assist was measured by Spagnol et al. (2012) at 105 W. A rider on an E-bike with a 1:1 torque control would thus provide about 50 W instead on the same ride and speed.

## 4.3 Bike sharing systems

Bike Sharing Systems (BSS) are systems with shared bicycles that can be accessed by users as a flexible mean of transportation. The number of systems set up is increasing each year and to date there are more than 600 cities around the world with BSS (ITDP, 2013, p. 10). The common system design is to have a dense network of stations spread out over a city making it possible to travel easily from one station to another (ITDP, 2013). The stations have three main components: Bicycles, docking spaces and a terminal (ibid.).



Figure 10. Example of BSS bikes and docking spaces. Source: Own work.

The characteristics of the bicycles are usually that they are sturdy unisex models, with a basket in the front or a rack for bags or other light goods (see Figure 10). The docking spaces are used to lock the bikes when they are not in use (Figure 10). Docking is usually performed by simply holding the bike against the docking pole and locking is performed automatically. The purpose of the terminal is from a user perspective to provide all necessary information about the system including check-in and payment functionality. The presented information can be how to check in and out bikes, how to pay or register, where the nearby stations are located and if there are available docking spaces or not. When a customer wants to start a journey, he or she register at the terminal and one of the bikes unlocks. Check-out functionality may be built into the docking poles as well.

As BSS are designed to provide flexible means of transport for many people, there is usually an economic incentive in place to discourage people to use the bikes for a long period of time. One example of pricing is the BSS Styr & Ställ Gothenburg. The first 30 minutes are free for yearly subscribers and the cost of going into the next 30 minutes period is 10 SEK, the next-coming 20 SEK and thereafter 40 SEK per half hour (JCDecaux, 2014). To sign up for one season (1st of March to 31th of November) costs 75 SEK if you connect your account to your public transport card (ibid.).

The terminals also play an important role for the operators. They keep track of when a user starts and stops a trip in order to bill for the correct amount of time. Another important indicator is the load factor, i.e. the number of bicycles per docking space. As the rides are inhomogeneous during the day, there will be stations that becomes empty or full of bikes. Both will cause problems for the user that either may want to use a bike and not finds one available, or want to return one and find the station full. To overcome this problem, the terminal sends information on the station's load factor to the operator's server. They can then use this information as decision support on how, when and where to redistribute bikes. Redistribution is mainly performed by flatbed trucks or vans with trailers (ITDP, 2013, p.

112). The cost of redistribution is a large share of the operating cost. In the case of Barcelona's BSS, it accounts for 30% (OBIS, 2011, p. 27). A second method to avoid full stations — and necessity for a system where bikes move between stations — is to build more docking spaces than there are bikes. ITDP's bicycle sharing planning guide (2013) recommends 2-2.5 docking spaces per bike. The figure is based on experiences from different BSS operators (ibid.). An indicator that can be used to evaluate the performance of one BSS compared to others is the number of trips per bike and day. Table 3 shows usage statistics for six different cities. There is a wide range of usage where Gothenburg being one of the lowest. The usage is dependent on many factors such as pricing and station locations.

**Table 3. Average number of trips per day and bike for a few cities with large-scale BSS (ITDP, 2013, p. 150; Trafikkontoret, 2012).**

City	Trips per bike and day
Gothenburg	1.3 (data only from 2012)
London	3.1
Paris	6.7
Barcelona	10.8
New York City	8.3
Washington, D.C.	2.4

The current BSS in Gothenburg is not operating the whole year. Their current operating season is from March 1 to December 31 (JCDecaux, 2014). This operational strategy is utilised around Europe in other cities with cold climate wintertime (OBIS, 2011, p. 31).

The total cost of a BSS varies depending on for example system design, pricing and operation. Two cities whose BSS profits differ a lot are London and Paris. The city of London subsidised their BSS, Barclays Cycle Hire, with about 118 million SEK in 2012. During the same year, Paris had a profit of 139 million SEK (Gladdis, 2013).<sup>4</sup> The reason for the success in Paris may be that the operator has landed a better sponsorship deal (ibid.) and that the system is used twice as much as London's system (see Table 3).

For large-scale BSS in Europe, it is estimated that the total investment cost is around 22 000-27 000 SEK per bike (OBIS, 2011, p. 26).<sup>5</sup> The largest share is the cost of building the stations (ibid.). In Barcelona for example, it accounted for 70% (ibid.). This share includes the cost of buying and installing the stations including all docking points and terminals. The second largest share of the investment cost is purchasing the bikes. In Barcelona, the bike investment accounted for 17% of the investment cost (OBIS, 2011, p. 26), i.e. approximately 1 900-3 100 SEK per bike with the average European investment cost from above.

<sup>4</sup> Conversion rate £1=10.75 SEK (2014-03-05)

<sup>5</sup> Conversion rate €1=8.84 SEK (2014-03-05)

When the system is up and running, there are operational costs such as redistribution and maintenance. The estimated operating cost for European BSS is about 13 000-22 000 SEK per bike and year (OBIS, 2011). The largest share of that being redistribution, followed by bike and station maintenance and administration (ibid.). Another factor that is important to consider in BSS is the health impact from cycling. Several studies have found the benefit of cycling to outweigh its risks (Oja, et al., 2001; de Hartog, et al., 2010; Rojas-Rueda, et al., 2011). Rojas-Rueda et al. (2011) estimate that the BSS in Barcelona reduces mortality by about 10-12 deaths/year. The main factor behind that was increased physical health of the users (ibid.). The health benefits of using BSS have been acknowledged by the city of Boston, which launched a program to prescribe subsidised subscription to the town's BSS to fight obesity (Malamut, 2014).

### **4.3.1 Taking the leap from BSS to E-BSS**

Using E-bikes in a BSS (E-BSS) could enable longer and hillier rides as the rider's effort is reduced. The stations could thus be placed further away from the city centre and encourage commuting by E-bikes in places BSS do not cover today. This would lead to a shift from other modes of transport available such as car or bus. The stations of E-BSS would be different to regular BSS. From a user perspective, the main difference would be E-bikes instead of regular bikes, but from an operator's perspective; much is changed. First of all, the E-bikes need to be charged, each docking space must thus be equipped with charging ability and a battery management system. If the E-bikes would have enough charge it could be possible to include some docking poles without charging ability as a means to reduce the cost. The poles must be designed in a safe way so that no voltage is applied to reachable parts in the docking pole. The terminal must also take the SOC of the E-bikes into consideration to ensure that the battery capacity is enough for the next trip. (This can of course be debated. An E-bike can be used as a regular bicycle if no power is available so it is a question of user experience.) The use of E-bikes also opens up for some interesting possibilities, as power is available on the bike. This can for example be to power a GPS to enable tracking of stolen bicycles or to gather data on speed and location for system optimisation and travel pattern research.

## 5. Methodology for calculations on a solar powered E-bike sharing pool

This chapter presents the methodology on how the system calculations are performed. It starts with solar power calculations in section 5.1, followed by E-bike calculations in section 5.2 and a combined system model in section 5.3.

### 5.1 Solar energy calculations

It is important to define a coordinate system that can be used consistently to be able to keep track of the position of the solar panel relative the sun and the urban surrounding.

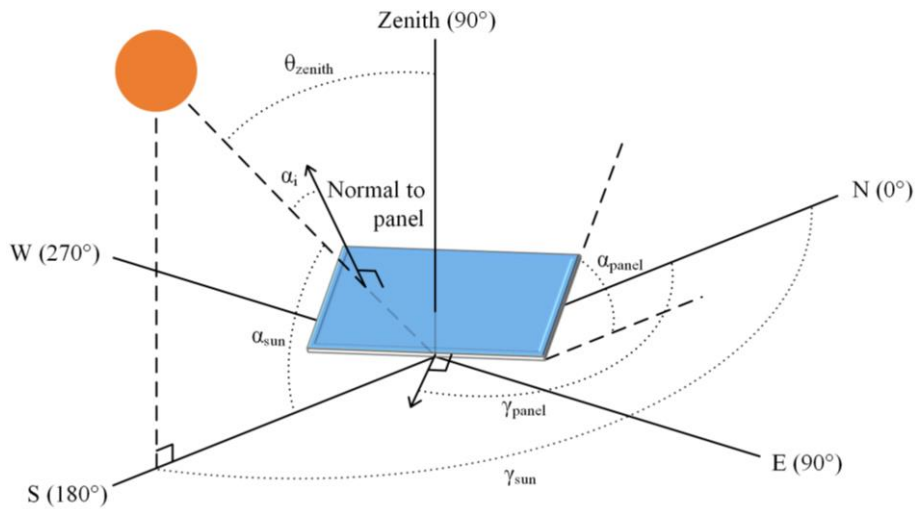


Figure 11. Definition of angles between the sun and a solar panel.  $\gamma$  indicates azimuth angles ( $0^\circ$  is north and  $90^\circ$ , east);  $\alpha_{sun}$  is the altitude angle of the sun and  $\alpha_{panel}$  the tilt angle of the panel, both relative horizon;  $\alpha_i$  is the angle of incidence between the direct irradiance and the solar panel's normal and  $\theta_{zenith}$  is the zenith angle (i.e.  $90^\circ - \alpha_{sun}$ ).

Figure 11 defines all the important angles for the sun and a solar panel.  $\gamma_{panel}$  and  $\gamma_{sun}$  notes the azimuth angle of the panel and the sun respectively, both are defined as  $0^\circ$  to north and  $90^\circ$  to the east;  $\alpha_{panel}$  and  $\alpha_{sun}$  notes the angle relative ground for the panel and the sun respectively;  $\alpha_i$  is the angle of incidence between the sun's direct irradiance and the normal of the solar panel and last is the zenith angle,  $\theta_{zenith}$ , which indicates the angle between zenith and the sun. The equation to calculate the angle of incidence is shown in Appendix 2, Equation A2.1.

#### 5.1.1 Irradiance data

Data of irradiance can either be obtained by ground or satellite measurements. Most of the irradiance used in this report comes from SoDa, a provider of irradiance and meteorological data (SoDa, 2014). Their data is derived from satellite measurements that are processed into different irradiation databases. The one used in this report is called HelioClim-3 (or HC3) and shows the hourly irradiation for all different irradiance components presented in Table 1 starting from 1st of February 2004 to 31st of December 2005. The data is constructed in such

way that during the first hour of a day (00:00-01:00), the irradiance is integrated and is recorded at 01:00. Each irradiation value thus represents the last hour. As the temporal resolution is set to one hour, the data may be seen as either the average irradiance during the last hour (e.g. 878 W/m<sup>2</sup>) or the integrated irradiation during the last hour (e.g. 878 Wh/m<sup>2</sup>). Datasets of different tilt and azimuth angles were requested from SoDa to enable analysis of the effect of different panel orientations. It was chosen to download datasets with azimuth from 90° (east) to 270° (west) with a 10° resolution. The tilt angle was then varied from 0° to 90° at a 5° resolution. An irradiation dataset was then downloaded for each configuration of azimuth and tilt.

In an ideal world, there would be no interruptions in the measurements and the data gathering. In reality, equipment may fail, data get corrupted due to low signal etc. This means that sometimes there will be gaps in the data. Another reason for missing data that applies specifically to HelioClim-3 is that it cannot estimate the irradiance when the sun's altitude angle is less than 12° (Thomas, 2013). This causes missing data wintertime on high northern latitudes such as Sweden. For the used data that occurred from November 27, 2004 to January 19, 2005 and November 24, 2005 to the December 31, 2005. An interpolation methodology to fill these gaps has been developed. This is done to be able to compute energy yields on the entire period without interruption. For further information on the interpolation see Appendix 3. The error of the interpolated data is within possible irradiation variation from NASA presented in section 4.1.1.

### 5.1.2 Case study on four possible station locations in Gothenburg

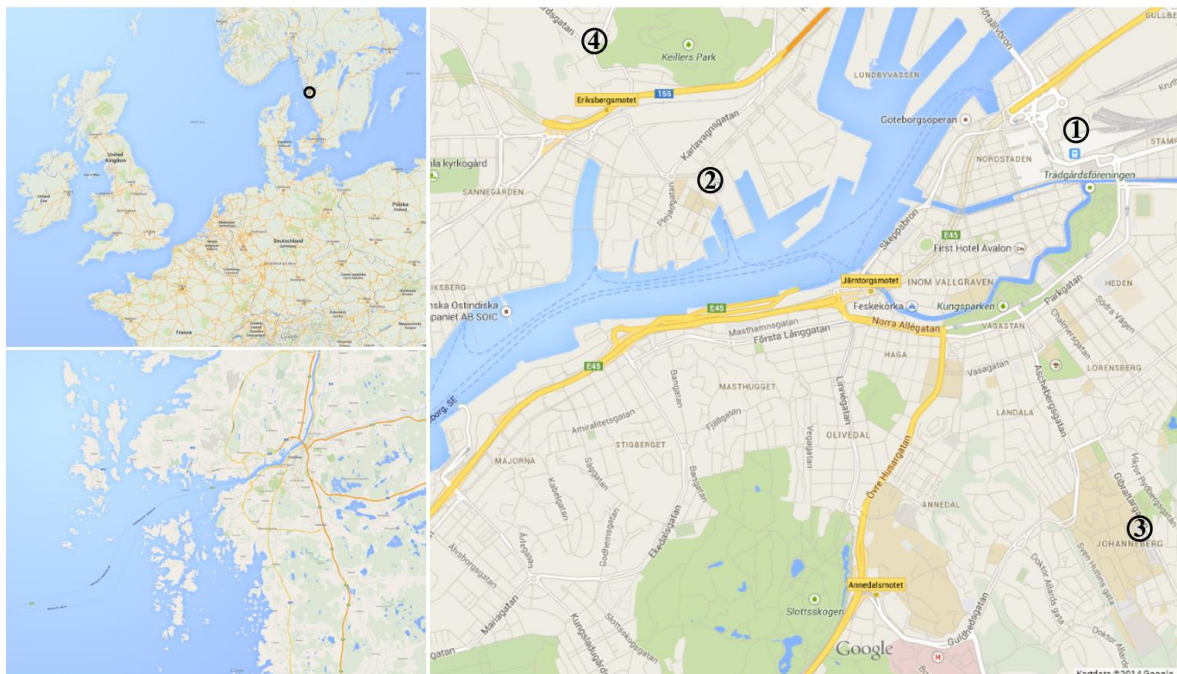


Figure 12. Overview images of the location of Gothenburg and the chosen locations for possible station placement. The names of the locations can be found in Table 4. Map data: ©2014, Google.

A case study on four potential station locations in Gothenburg is performed in order to study how varying city landscape affects the available solar energy. The chosen locations are presented on a map in Figure 12. The names of the locations and the respective reason of choice are presented in Table 4. Only the station at Lindholmen will be presented in detail in the results section to decrease its length and results for the other stations may be found in appendix.

**Table 4. Investigated locations in Gothenburg, Sweden for solar PV calculations. A map of the locations is shown in Figure 12.**

Location <sup>a</sup>	Reason for choice of location
1. Central Station	Major traffic hub in Gothenburg. Future possible station location within the research project Elmob at Viktoria Swedish ICT.
2. Lindholmospiren	Area in Gothenburg with many offices and thus commuters. Also a possible E-bike station within the Elmob research project at Viktoria Swedish ICT.
3. Chalmers University of Technology	Technical university, a new electromobility hub will be built as a fully electrified bus line starts in 2015 within the research project Electricity. An E-BSS could serve as an extension to the bus line.
4. Gropegårdsgatan	Close to Volvo Group's headquarter with poor connection to Lindholmospiren

<sup>a</sup> Precise coordinates of the locations: Central Station (57.71012°N, 11.97369°E), Lindholmospiren (57.70758°N, 11.93831°E), Chalmers Library (57.68997°N, 11.97921°E), Gropegårdsgatan (57.71458°N, 11.92667°E).

### 5.1.3 Losses in the solar cell

Apart from the solar cell conversion efficiency discussed in section 4.1.2 there are additional losses that takes place in reality and will be presented in this section.

Due to the nature of semiconductors, there will be an increase in internal resistivity of a solar cell with increased cell temperature (Rauschenbach, 1980, p. 74). Commonly, the response of this is referred to as the Temperature Coefficient (TC) in solar panel datasheets. Typical TC values for crystalline solar panels is around -0.3 %/°C to -0.5 %/°C relative 25 °C (Skoplaki & Palyvos, 2009). If the cell temperature is higher than 25 °C, the solar panel will thus generate less power than its nameplate states. This is often the case as the more irradiance, the higher the cell temperature. Various simplified models have been presented to estimate the solar cell temperature based on a number of different parameters (Jakhrani, et al., 2011). The used method in this report was presented by Garcia and Balenzategui (2004) and is presented in detail in Appendix 2, A2-5. Temperature data was collected from the Swedish Meteorological and Hydrological Institute, SMHI (2014).

Despite the use of anti-reflective coatings on solar panels front glass, there will still be reflections causing irradiance loss (Martin & Ruiz, 2001). These are taken into account in the

calculations by a methodology presented by Martin and Ruiz (2001) for the direct and diffuse irradiance respectively. For further information see Appendix 2, A2-3.

The proverb: '*A chain is not stronger than its weakest link*' is unfortunately true for solar panels. As a solar panel is constructed by series-connected cells, if only one cell is shadowed, the whole panel's output will change drastically. This does not only affect the power output but also puts the panel at risk as the shaded cell will start to dissipate power (Rauschenbach, 1980, p. 77). The easiest way to deal with this is to design the system so that series connections are avoided as much as possible. By parallel connecting panels and adding a blocking diode on each panel, you prevent the whole system to be affected if one panel is partially shaded. This will however not solve the problem with individual panels losing much of their power during partial shading, as often will be the case in urban environment. A possible solution is to employ diodes at strings of cells or even at each cell; but as panels are enclosed they must be manufactured in such way.

Solar cells — especially those made of crystalline silicon — experience significant drop in efficiency in low-light conditions (Reich, et al., 2005). However, the effect of accumulated energy yield is low and due to this reason, this effect is not be considered in this report.

#### **5.1.4 Shading in the urban environment**

Placing solar panels in an urban environment will introduce shading by nearby buildings and trees. Detailed analysis requires complex three-dimensional modelling in order to assess the irradiance on each part of a solar panel. To reduce the complexity, both in data collection and calculations, the shading is estimated at a single point and then assumed to be homogenous on the whole PV system.

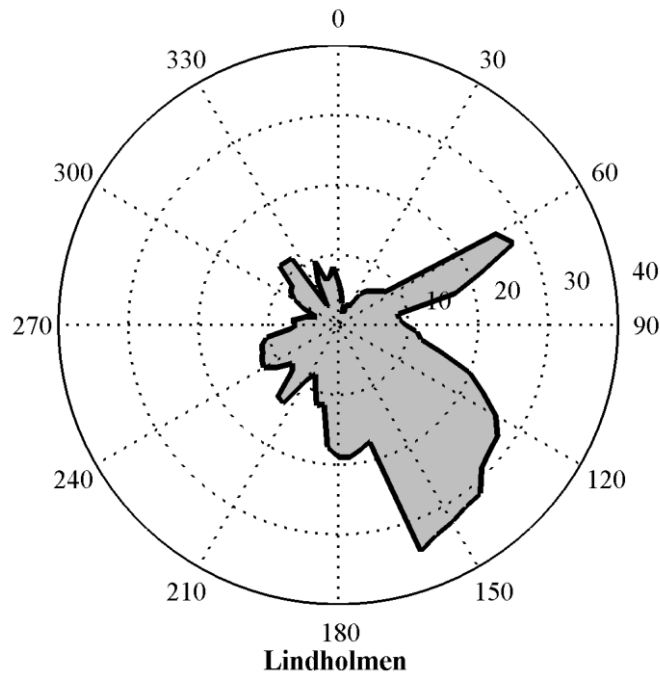


Figure 13. Polar plot of a horizontal profile measured at Lindholmen. The circle marks the azimuth angle ( $^{\circ}$ ) and the radius from the centre the altitude angle relative horizon ( $^{\circ}$ ). Note that  $180^{\circ}$  is south which means that buildings around  $180^{\circ}$  will be most important for the loss of incoming irradiation.

As the city landscape is different wherever you go, it is important to model the landscape where the panels are to be placed in order to be able to estimate shadowing losses properly. A way to measure the horizon is to stand on the point where the panels are to be mounted and note the azimuth and altitude angle for the skyline  $360^{\circ}$  around. In order to estimate if there will be any direct irradiance or not, it is possible to compare the sun's location with the profiling curve of the location's skyline and see if the sun disk is shaded or not. The sun's location will be determined using the methodology presented by Reda and Andreas (2008). An example of horizontal profiling is shown in Figure 13. Further graphs are shown in Appendix 2 A2-4 for all locations presented in Table 4.

The next step is to estimate the loss of diffuse irradiance, which can be done by using the so-called sky view factor. It is the fraction of the hemisphere that is occupied by sky. A methodology to calculate the sky view factor from a horizon profile is given by Matzarakis and Matuschek (2011), see Appendix 2. By multiplying the diffuse irradiance that would have fallen onto a shadow-free solar panel with the sky view factor you thus get the amount of diffuse irradiance that would have fallen onto the panel at the investigated location. The sky view factor for the urban environment in Figure 13 is 0.93, which means that 7% of the diffuse irradiance is lost under the assumption that the diffuse irradiation is homogeneously distributed across the hemisphere.

### 5.1.5 Specifications on the solar panel installation

One of the main specifications to be defined is the roof area available per E-bike. The number of panels that fits on a roof above an E-bike station depends on the number of docking spaces and the roof margin wanted outside of the E-bikes. To get specifications on commercial solar panels, a short review was performed on six different solar panel manufacturers: Latitude Solar, SunTech Power, Q-Cells, SweModule, Panasonic and Yingli. The two most common panel sizes found were 1.67x1 m<sup>2</sup> and 1.96x1 m<sup>2</sup>. A part of the function of the solar installation can be to provide weather protection for the E-bikes. The installation should thus be sized so that the panels cover the E-bikes in a good way. A bicycle is approximately 1.5 m long but when a panel is tilted, its horizontal length will decrease. In order to cover the bike with solar panels tilted at for example 40°, the horizontal length needs to be 1.96 m. Looking at the panel sizes presented earlier, a depth of 2 m is assumed for the solar panels. The width of the installation depends on the number of docking points and the space between each pole. That distance is approximated to be 0.7 m. A station with 15 E-bikes would thus be 11 m wide including a small margin on each side. The area of solar panel per docking space would in that case be almost 1.5 m<sup>2</sup>/docking space. With the BSS system design figure of 2-2.5 docking spaces/bike presented in section 4.3, that converts to a maximum area of 3-3.8 m<sup>2</sup> solar panel per E-bike. The electrical output from the solar panels will depend on the solar cell technology chosen. The panels are assumed to be fixed as tracking would be tricky to accomplish in an urban environment. Table 5 presents the assumed parameters for the calculations on the available electric energy from the solar panels. The specifications are representative for solar panels of high quality.

**Table 5. Set specifications for the calculations of available electric energy.**

<b>Solar installation specifications</b>	
Solar cell technology	Multi-junction
Panel efficiency	19%
Temperature Coefficient (TC)	-0.29%/°C
NOCT value	44 °C
Maximum solar panel area per E-bike	3-3.8 m <sup>2</sup>

## 5.2 Modelling an E-bike

This section focuses on the E-bike's power and energy use. Newton's second law of motion states that,

$$ma = \sum_i^n F_i, \quad (3)$$

where  $m$  in the case of an E-bike is the total mass of the rider and the E-bike (kg),  $a$  the acceleration (m/s<sup>2</sup>) and  $F$  all the different forces (N) that affects the E-bike. When riding in constant speed there are three forces counteracting the input forces that needs to taken into

account: Air-drag, rolling resistance and climbing force. The sum of the forces for an E-bike in constant speed is,

$$F_{human} + F_{motor} = F_{air} + F_{roll} + F_{climb}. \quad (4)$$

where  $F_{human}$  is the force provided by pedalling,  $F_{motor}$  the force provided by the electrical motor,  $F_{air}$  the air drag,  $F_{roll}$  the rolling resistance and  $F_{climb}$  the force when climbing up- or downhill. The power (W) is the force times velocity,

$$P = Fv \quad (5)$$

where  $v$  is the speed relative ground (m/s). If the input power is larger than the total losses, the bike will accelerate until the equation is balanced. The following sections will present each force and as well as the energy use during acceleration.

### 5.2.1 Power during acceleration and deceleration

Energy is stored in momentum of the rider. The stored energy of a moving object can be expressed as,

$$E = \frac{1}{2}mv^2, \quad (6)$$

where  $E$  is the energy in Joules,  $m$  the mass (kg) and  $v$  its velocity (m/s). The energy needed to accelerate an object from velocity  $v_0$  to  $v_1$  is thus,

$$\Delta E = \frac{1}{2} \cdot \frac{1}{3.6 \cdot 10^3} m(v_1^2 - v_0^2), \quad (7)$$

where  $\Delta E$  is the energy needed in Wh. Accelerating an E-bike with the total mass of 100 kg from 0 km/h to 25 km/h will for example need 0.7 Wh provided to the road excluding all other forces. The power used during the acceleration depends on the time of acceleration which is limited by the power the human and the electric motor may supply.

### 5.2.2 Power to overcome air drag

One of the forces that is especially strong in high speeds is wind resistance. Its power may be expressed as,

$$P_w = \frac{C_d \rho A}{2} (v_w + v_g)^2 v_g, \quad (8)$$

where  $C_d$  is the coefficient of air drag,  $\rho$  the air density<sup>6</sup> (kg/m<sup>3</sup>),  $A$  the total area of the rider and the bicycle as seen from the front (m<sup>2</sup>),  $v_w$  the head wind speed (m/s) and  $v_g$  the ground

<sup>6</sup> Can be approximated by  $\rho = 1.2e^{-0.143h}$  where  $h$  is the elevation above sea level in km (Morchin & Oman, 2006).

speed (m/s) (Morchin & Oman, 2006, p. 24). A typical value for the coefficient of air drag is 1 for an upright cyclist (Morchin, 1996), which is assumed to be the seating position for E-bikes in an E-BSS. The frontal area can be assumed to be 0.50 m<sup>2</sup> (measured by Morchin and Oman (2006) for a male weighing 80 kg). Note that the wind speed marks the head wind speed. Cycling north when the wind speed is 5 m/s from northeast will for example result in a 3.5 m/s head wind speed due to the 45° displacement. Wind coming from the back of the rider is represented by negative values.

### 5.2.3 Power to overcome rolling resistance

The rolling resistance is caused by the tires, bearings and other moving parts on the bicycle. It is thus dependent on the bicycle design but also its speed and the total weight of the rider and bicycle. The power needed to overcome the rolling resistance is,

$$P_{roll} = gC_r m_{tot} v_g, \quad (9)$$

where  $g$  is the gravitational acceleration (9.81 m/s<sup>2</sup>),  $C_r$  the coefficient of rolling resistance,  $m_{tot}$  the total mass of the rider and bicycle (kg) and  $v_g$  the speed relative ground (m/s) (Morchin & Oman, 2006, p. 26). The coefficient of rolling resistance for an E-bike and a rider ( $m_{tot}$  at 99 kg) has been measured to 0.0071 on smooth asphalt by Morchin (1996).

### 5.2.4 Power during climbing

When riding up- or downhill there are changes in potential energy that need to be accounted for. An expression for the power during climbing is,

$$P_{hill} = g m_{tot} v_g G, \quad (10)$$

where  $g$  is the gravitational acceleration (9.81 m/s<sup>2</sup>),  $m_{tot}$  the total weight of the rider and the bicycle (kg),  $v_g$  the speed relative ground (m/s) and  $G$  the road grade (%) (Morchin & Oman, 2006, p. 23). The road grade can for small hills be approximated as the fraction between the rise and the bird's eye distance travelled. For steep hills it may be computed by,

$$G = \sin(\tan^{-1}(\frac{\Delta h}{\Delta l})), \quad (11)$$

where  $\Delta h$  is the height difference of the hill and  $\Delta l$  the horizontal distance; both in meters. Note that  $G$  is positive uphill, negative downhill and zero in flat conditions. Table 6 shows examples of the slope grades for three steep roads in Gothenburg. Going uphill on Aschebergsgatan in 20 km/h would for example require 245 W in pure hill climbing power for rider weighing 75 kg with a 25 kg E-bike.

**Table 6. Examples of slope grades for three roads in Gothenburg.**

<b>Road name</b>	<b>Subsection</b>	<b>Length (m)</b>	<b>Slope (%)</b>
Aschebergsgatan	Vasaplatsen-Chalmers University of Technology	650	4.5
Stigbergsliden	Barlastgatan-tram station at top	180	6.5-7.0
Göta Älvbron (bridge connecting to Hisingen)	North side to top	350	4.1

### **5.2.5 Regenerative braking**

It is possible to utilise the same method for energy regeneration on E-bikes as on hybrid cars. The main strategy in a hybrid car is to store energy that otherwise would be wasted as heat. When braking a vehicle with regeneration, instead of using regular friction brakes, an electric motor is activated that acts as a generator and supplies power to a battery. In this way, it is possible to store energy when for example stopping at traffic lights or going downhill. The amount of recoverable energy is however questionable on E-bikes. Morchin and Oman (2006) computed that the recoverable energy on an E-bike was about 1.3% of what was used. One reason for the low value can be differences in rider characteristics between cyclists and drivers. When you supply power of your own you get more energy efficient by for example trying to glide towards a red light hoping for it to turn green in time. Another issue can be that there is a difference in speed up- and downhill for cyclists. A car usually has about the same speed up- and downhill to follow speed regulations. When cycling however, people are used to go slow uphill and fast downhill. It may thus be the case that it is preferred to ride in high speeds downhill and let the wind resistance act as one of the main braking forces instead. In such case, there would be low energy available for regeneration. It is not common to have regeneration on E-bikes today as it requires more complex motor control (Muetze & Tan, 2007). As few E-bikes with regenerative braking are available on the market, it however assumed that E-bikes for a pool project will use friction brakes only.

### 5.3 Modelling an E-BSS system

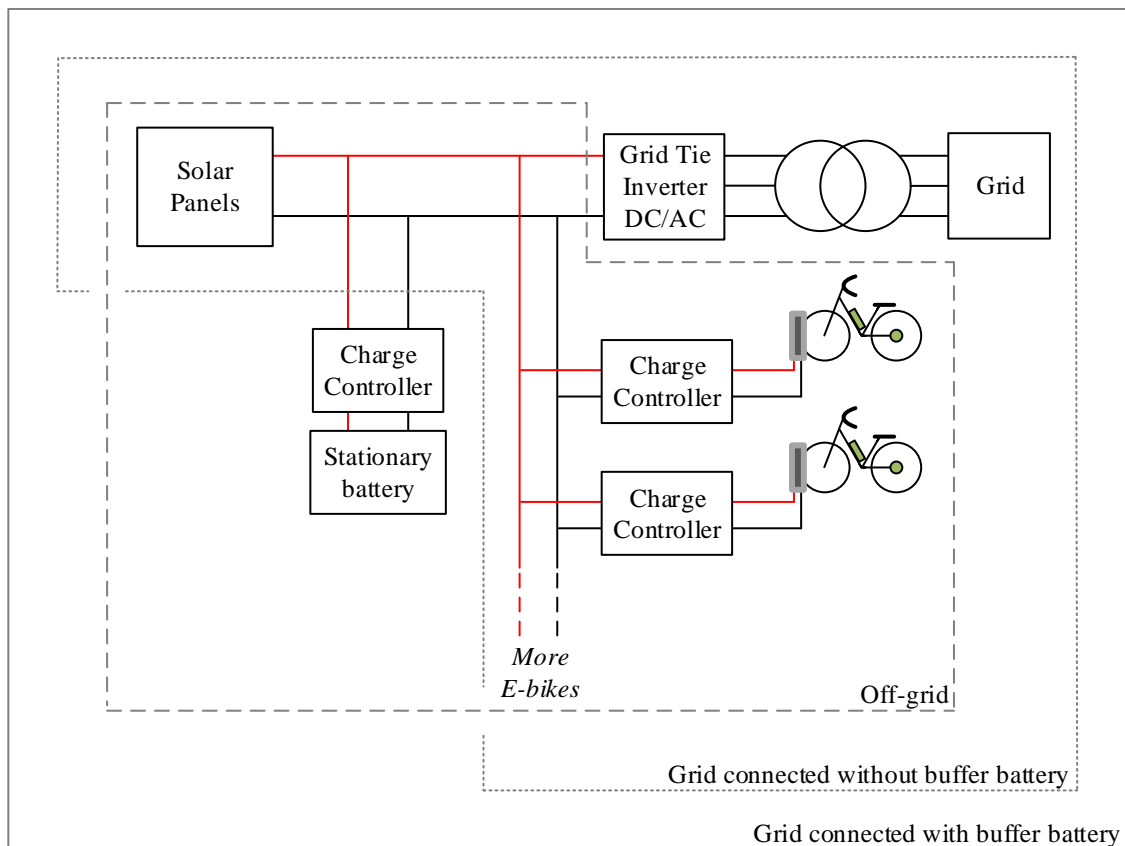


Figure 14. Examined electric system layouts of the E-BSS.

Three different system layouts have been studied as shown in Figure 14; two on-grid solutions and one off-grid. The off-grid solution consists of solar panels, a buffer battery and one charge controller for each E-bike. The on-grid solutions also include a DC/AC inverter for connection to the grid and either a buffer battery or not. Some advantages and disadvantages of the system layout options are presented in Table 7.

Table 7. List of advantages and disadvantages for the different system layouts.

Solution	Advantage(s)	Disadvantage(s)
Off-grid	Mobile solution is possible No ground work is needed	Excess solar energy cannot be utilized fully Large stationary battery and solar panel area is needed for stable operation at all times
On-grid without buffer battery	Easy solution	Grid exchange will be high
On-grid with buffer battery	Solar energy can be stored and grid exchange minimised	Complex solution

The energy requirements during operation of an E-BSS will depend on how many trips are made, how long they are and how the E-bikes are designed and used. Some data is available

on average use rates for European BSS (ITDP, 2013, p. 150) but to make an hourly assessment, more detailed data are needed.

The U.K. government Transport for London have published statistics on usage of London's BSS (Transport for London, 2014). The dataset includes several million individual hires and their start and end station and time. From that dataset, 4.3 million hires were analysed from the 25th of August to the 31st of December, 2012. The average amount of trips per bike and hour throughout a day was computed from this dataset. As the usage characteristics varied quite a lot between weekdays and weekends, their respective hourly average usage were analysed separately. Once the hourly usage was extracted for weekends and weekdays, they were combined into a matrix with the same size as the hourly incoming solar irradiation. That is, hourly values from February 1, 2004 to December 31, 2005. By doing so, it is possible to do hour by hour calculations on the electric energy from the solar panels and the energy that is required to power the E-bikes. However, there are great variations in the average daily use between cities' BSS. London's average is for example 3.1 trips per bike and day and other cities have more than three times that (see Table 3). In order to make system calculations with good safe margin, it was chosen to scale the usage data from London to match the town with the highest average trip usage known for a European BSS, i.e. Barcelona with 10.8 trips per bike and day.

What also needs to be assumed for energy calculations on an E-BSS, is how the trips are made. In order to assess the impact of the energy requirement, three different rider profiles were created. The three profiles are called tourist, casual rider and commuter (see Table 8). The tourist rider is assumed to ride in a slow pace, have many stops and also stop for a longer time than the other two rider styles. The casual rider is assumed to be an inner-city rider that uses the bike to move from point A to B, but makes a stop to for example enter a food store on the way. Finally, the commuter rides at high speed and make few stops during the trip. The trip length was assumed to be for all rider profiles. The road was set to have three segments, each with a different slope: 0.5 km at 5% slope, 1 km at 1% slope and 3.5 km at 0% slope. The wind speed was set to 2 m/s headwind.

**Table 8. Assumed specifications for three different rider profiles.**

<b>Rider style</b>	<b>Average speed (km/h)</b>	<b>Number of full stops per (km)</b>	<b>Time without moving per trip (min)</b>
Tourist	15	4	20
Casual	20	2	15
Commuter	25	1	0

The remaining constants can be found in Table 9 of which most have been presented in earlier sections. The electric energy needed from the battery was computed using equations 6-11. To compute the average E-bike's battery level at the end of each hour, several steps were

performed. Note that all of the following equations were computed per hour unless anything else is stated. First, the available charging time was computed as,

$$t_{charge} = n \left( 1 - (vs + t_{stop}/60) \right), \quad (12)$$

where  $n$  is the number of trips per bike during the investigated hour,  $v$  the average speed (km/h),  $s$  the distance (km) and  $t_{stop}$  the stop time (min). As the charging time cannot be negative, all computed  $t_{charge} < 0$  was set to zero. Such occasions can be during peak-hours when the use is very high and there might thus not be any substantial charging time available. The average hourly energy (Wh) needed for the trips made was computed by,

$$E_{trip} = E_{trip\ style(i)} n \quad (13)$$

where  $E_{trip\ style(i)}$  is the energy needed per trip (Wh/trip) for each rider style (computed using equations 6-11, Table 8 and Table 9) and  $n$ , the number of trips that hour (trips/(hour & bike)).

**Table 9. Constants used in the calculations of the E-BSS.**

Constant	Value	Unit
Mass of rider	75	kg
Mass of bike	25	kg
$C_d$ (air-drag coefficient)	1	-
$C_r$ (rolling resistance coefficient)	0.0071	-
$A$ (frontal area)	0.5	m <sup>2</sup>
$h$ (elevation above sea)	15	m
Electric to human power	1:1	
Motor efficiency	80	%
E-bike electronic efficiency	94	%
Battery voltage	36	V
Battery capacity	10	Ah
Charger power (about 2 A)	70	W
Charger efficiency	90	%
Average trip distance	5	km

The maximum energy (Wh) that there is time to charge per hour is,

$$E_{max\ charge} = t_{charge} P_{charger}, \quad (14)$$

where  $t_{charge}$  is the available charging time (h) each hour and  $P_{charger}$  the power supplied by the charger to the battery (W). The battery level (Wh) is now computed as,

$$E_{battery}^*(i) = E_{battery}(i-1) - E_{trip}, \quad (15)$$

where  $E_{battery}(i)$  is the battery capacity at the  $i$ :th hour,  $E_{battery}(i-1)$  the battery capacity the previous hour and  $E_{trip}$  the energy needed for the trip. This computed battery level thus

corresponds to the level just after the trip has finished and before the charging has begun. As the battery level cannot become negative,  $E_{battery}$  was set to zero for those cases. That indicates a battery depletion, which would lead to a user having to use the E-bike as a regular bicycle a part of the trip. The energy needed for the battery to become fully charged can be computed by,

$$E_{to\ full\ charge} = E_{total\ battery\ capacity} - E_{battery}. \quad (16)$$

Now there are two cases to consider. If the energy to full charge is lower than the maximum available charging energy, the battery will be charged to full charge and otherwise, it will be charged by the maximum charging energy available. The energy needed to each E-bike from the power supply is thus,

$$E_{supply} = \begin{cases} E_{to\ full\ charge}/\eta_c & \text{when } E_{to\ full\ charge} < E_{max\ charge} \\ E_{max\ charge}/\eta_c & \text{when } E_{to\ full\ charge} \geq E_{max\ charge} \end{cases}, \quad (17)$$

where  $\eta_c$  is the charger efficiency. The average battery level at the end of the hour is thus,

$$E_{battery}(i) = E_{battery}^*(i) + E_{supply}\eta_c. \quad (18)$$

Equations 14-18 are used to compute the average battery level under the assumption that the charging energy is always available.  $E_{supply}$  depend on the system configuration but can be computed by,

$$E_{supply} = E_{solar} + E_{stationary\ battery} + E_{grid}, \quad (19)$$

where  $E_{solar}$  is the energy from the sun ( $\geq 0$  Wh/h),  $E_{stationary\ battery}$  the energy from the stationary battery and  $E_{grid}$  the energy to ( $>0$ ) or from ( $<0$ ) the grid and. An off-grid solution would exclude the grid energy exchange and perhaps even the stationary battery depending on configuration. The solar energy remains uncontrolled but the grid and the stationary battery may be controlled in a desired way. One example could be that an on-grid system with a stationary battery should utilise the battery at its maximum to minimise the grid exchange. By combining such control strategy with equation 19 it is possible to compute each parameter for each hour.

## 6. Results

This section shows the result of the calculations on an E-BBS. The section is divided into three subchapters for the solar calculations, E-bike calculations and system modelling respectively. To reduce the length of this chapter only the shadow-free case and the station at Lindholmen will be presented. Results from the other stations can be found in appendix referred to in each chapter.

### 6.1 Available solar energy and weather

This chapter present graphs and data from the calculations on the solar panels.

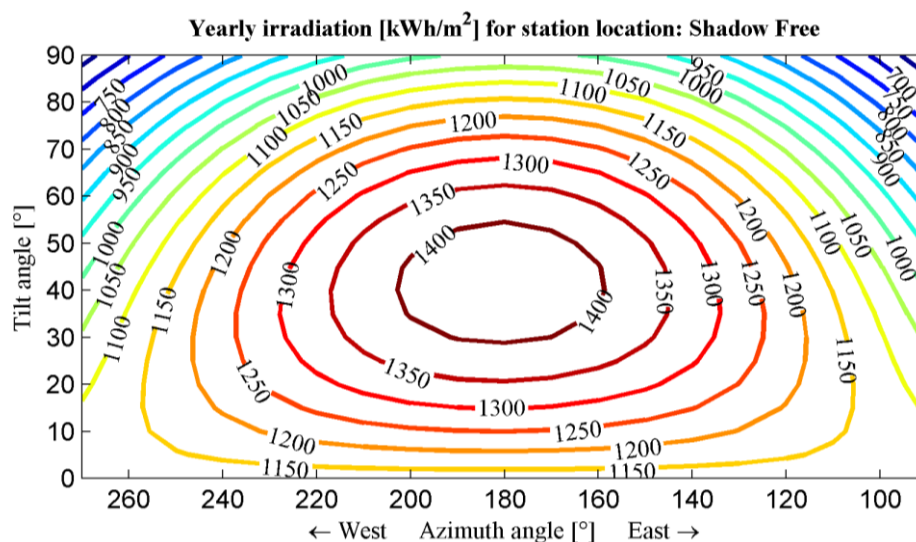


Figure 15. Yearly irradiation per m<sup>2</sup> for a surface with different fixed tilt and azimuth angles for a shadow-free surface in Gothenburg, Sweden.

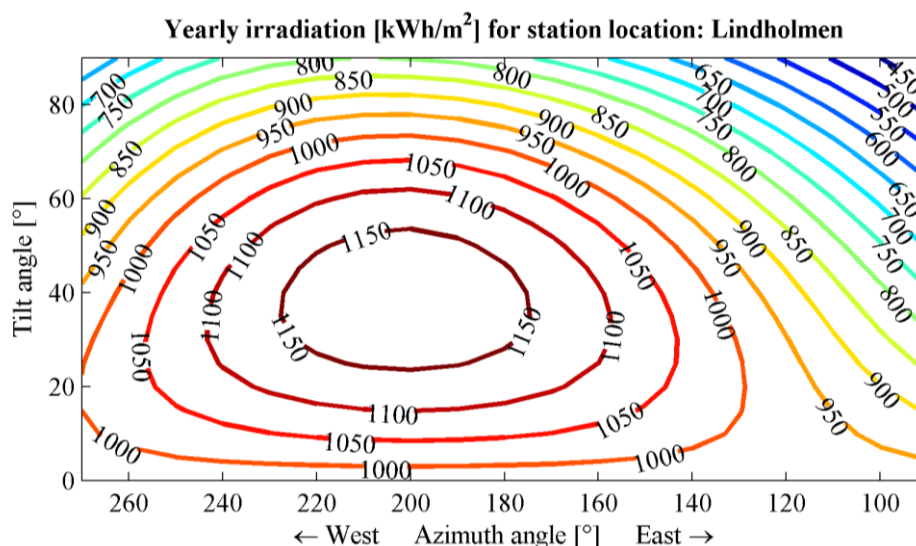


Figure 16. Yearly irradiation per m<sup>2</sup> for a surface with different fixed tilt and azimuth angles for a surface at Lindholmen in Gothenburg, Sweden.

Figure 15 and Figure 16 shows the yearly irradiation for different azimuth and tilt angles for a shadow-free location and one at Lindholmen (see Appendix 4 for the other locations). A first thing that can be noticed in both graphs is that the yearly irradiation is more dependent on the tilt angles than azimuth angle (the axes are to scale). Also, the optimum panel orientation differs between the cases. For the shadow-free case (Figure 15), the maximum irradiation can be found at  $180^\circ$  azimuth; i.e. south and a tilt around  $40^\circ$ . At Lindholmen (Figure 16), the optimum can be found more westwards around  $200^\circ$  azimuth and the same tilt. This is due to a building in the east that shadows the morning sun, and catching the afternoon sun from the west is thus more important. What also can be noted is that the maximum yearly irradiation at Lindholmen (Figure 16) has decreased compared to the shadow-free case (Figure 15) due to shading from nearby buildings.

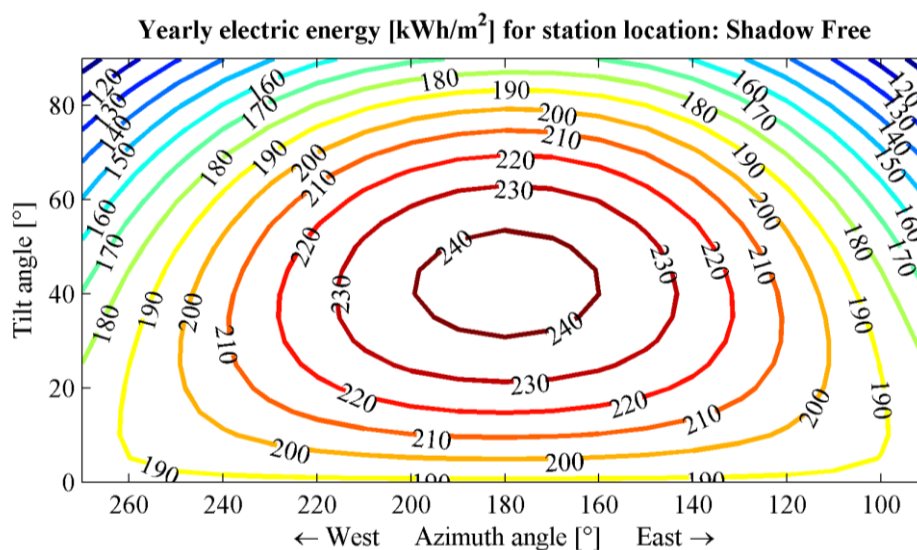


Figure 17. Yearly electrical energy yield for a solar panel placed on a shadow-free surface with different tilt and azimuth angles.

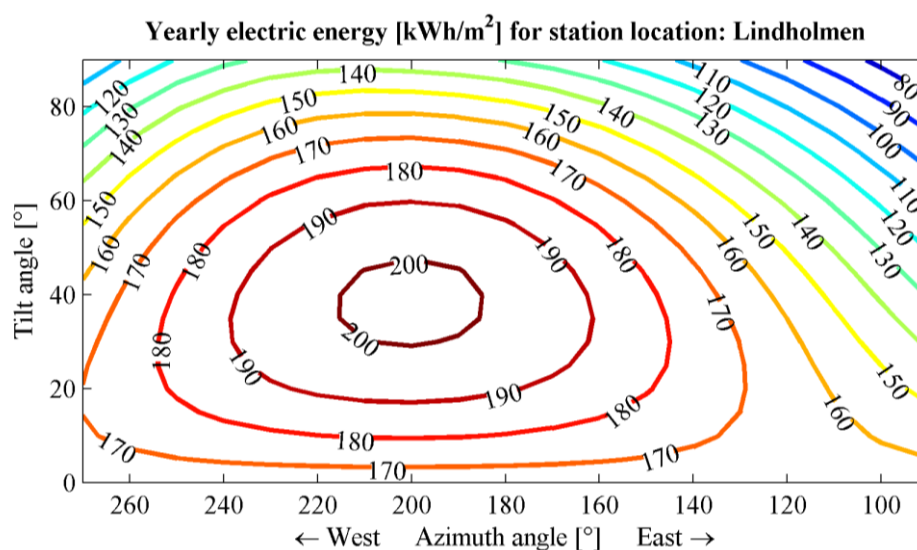


Figure 18. Yearly electrical energy yield for a solar panel at the Lindholmen station with different tilt and azimuth angles.

The electric energy yields are presented in Figure 17 and Figure 18. Note that they have been computed hourly and not on the yearly data presented in Figure 15 and Figure 16. However, the characteristic is more or less the same as for the irradiation.

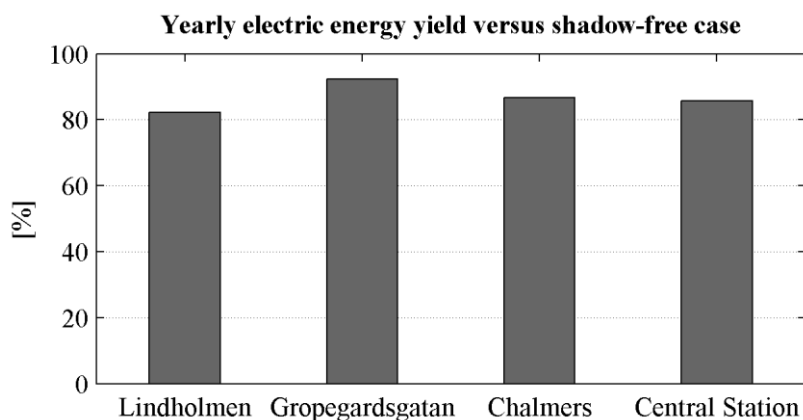


Figure 19. Yearly electric energy yield for the investigated station locations relative the shadow-free case.

Figure 19 shows the maximum electrical energy yield for the solar panels relative the optimal fixed orientation for a shadow-free surface. What can be seen is that about 15% of the yearly irradiation is lost. This means that even though there are buildings present, there is still good potential for solar panels in the urban environment. A way to further increase the incoming irradiance – and hence the electric energy yield – is to follow the sun. It was shown that tracking in the azimuth direction could increase the yearly irradiation by about 7% relative the optimum fixed orientation and 2-axis tracking, about 37%. However, tracking may not be possible in an urban setting where space is limited and tilting may reduce the panels ability of weather protection.

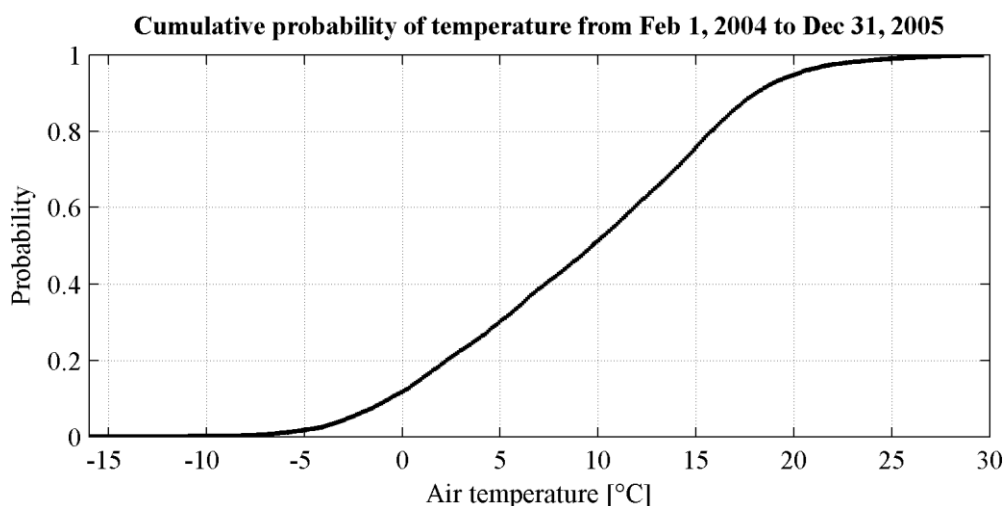


Figure 20. Cumulative probability of the air temperature in Gothenburg, Sweden from Feb. 1, 2004 to Dec. 31, 2005. Data from SMHI (2014).

The air temperature will have an effect on the use of the E-bikes but also the battery charging. In Figure 20, it can be seen that the temperature drops below 0°C around 10% of the time during which no charging is possible without battery heating. The charging current should be reduced below 5 °C and that corresponds to 30% of the time. If operation should be possible throughout the year it is thus important to include battery heating in some way.

## 6.2 E-bike electric energy use

Table 11 shows the energy required from the battery (Wh/km) for different sets of speed, wind speed and slope. The colour notes the effort by the rider in each condition and the values are computed for a 1:1 torque setting, meaning that the same amount of human and electrical power is used in each time instant. The remaining constants are noted below the table. Missing values indicate conditions where the calculated average motor power exceeds the limit (>250 W) and is thus not possible to obtain for long periods of time. If that occurs, the rider would simply lower the speed. It can be seen in Table 11 that the electric energy usage varies depending on the external factors. Values between 3-18 Wh/km were computed but around 5-10 Wh/km can be seen for typical cycling at high-speed. Note that these values are computed for constant speed. Including accelerations would increase the energy provided from the battery. The computed energy use from the rider profiles are shown in Table 10. The underlying assumptions were high total mass (100 kg), 5 km trip length with different steep segments, energy for full stops, etc.

**Table 10. Energy use, range and trip time for the rider profiles.**

<b>Rider style</b>	<b>Battery energy use (Wh/km)</b>	<b>Range at full battery (km)</b>	<b>Total trip time incl. stops (min/5 km)</b>
Tourist	5	70	40
Casual	6	60	30
Commuter	7	50	12

**Table 11. Calculated energy required from battery per distance travelled.**

Average E-bike speed (km/h)	Head wind speed (m/s)				Slope grade (%)
	0	2	4	6	
15	3	4	5	7	0
	6	7	9	11	2
	10	11	13	15	4
	13	15	16	18	6
20	4	5	7	9	0
	7	9	11	13	2
	11	12	14	16	4
	14	16	-	-	6
25	5	7	9	11	0
	8	10	12	-	2
	12	14	-	-	4
	-	-	-	-	6
Colour code represents level of effort by rider (human power, W)			Easy <100	Moderate 100-150	Hard >150

Assumptions: Mass of rider and E-bike 100 kg, motor control: Torque control 1:1 (electric to human power),  $C_d=1$ ,  $A=0.5 \text{ m}^2$ ; efficiencies: Motor 80%, E-bike electronic 94%;  $C_r=0.0071$ , two full stops per km, maximum motor power 250 W. '-' means that the maximum motor power is exceeded (in reality this can occur for short periods of time).

### 6.3 E-BSS energy results

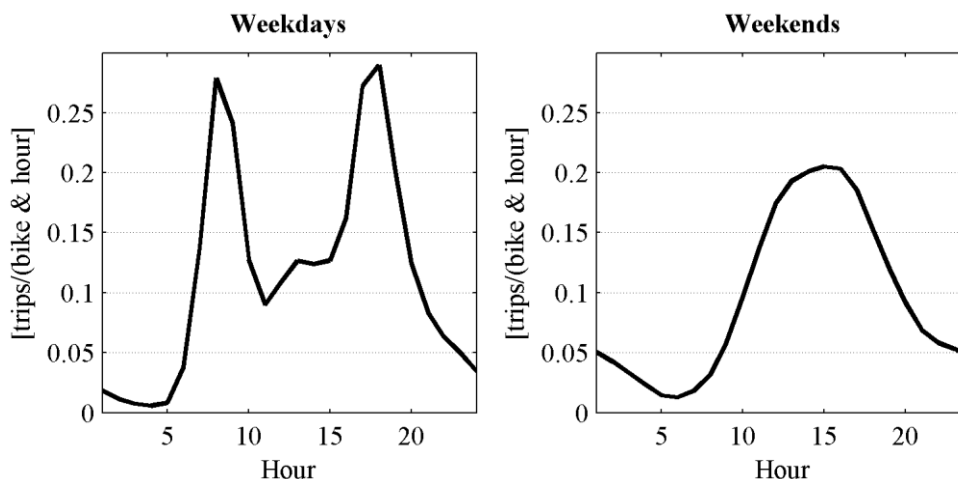


Figure 21. Average hourly bike usage for London's BSS for weekdays and weekends.

The usage profile for London's BSS is shown in Figure 21 for weekdays and weekends. The data is the average usage from the 25th of August to the 31st of December, 2012. What can be noted for weekdays are two distinct peaks when people commute to and from work. During weekends, the use is much more evenly distributed with the maximum usage in the afternoon.

It was computed that the average daily use was 2.6 trips/(bike and hour) for the studied period and that the maximum was 5.6 trips/(bike and hour).

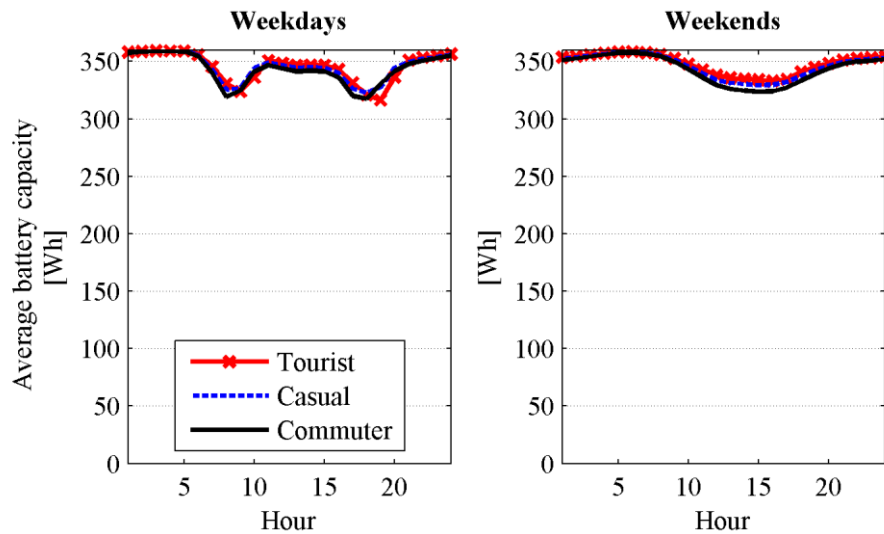


Figure 22. Average battery capacity (Wh) for an E-bike during weekdays and weekends for three different rider profiles and usage at 10.8 trips/(hour and day). The calculations are assuming that energy is available for charging when needed, i.e. a grid connected system. Note that the values represent the average battery level at the end of each hour, i.e. after the battery has been charged the time possible.

Figure 22 shows the result of the average battery capacity from simulations on a grid-connected system (with or without a stationary battery). Note that the values represent the value at the end of each hour. The battery level will thus be the lowest just after the trip has finished. Note also that this is the average battery level, which means that individual bikes will have even lower battery levels after a trip has finished.

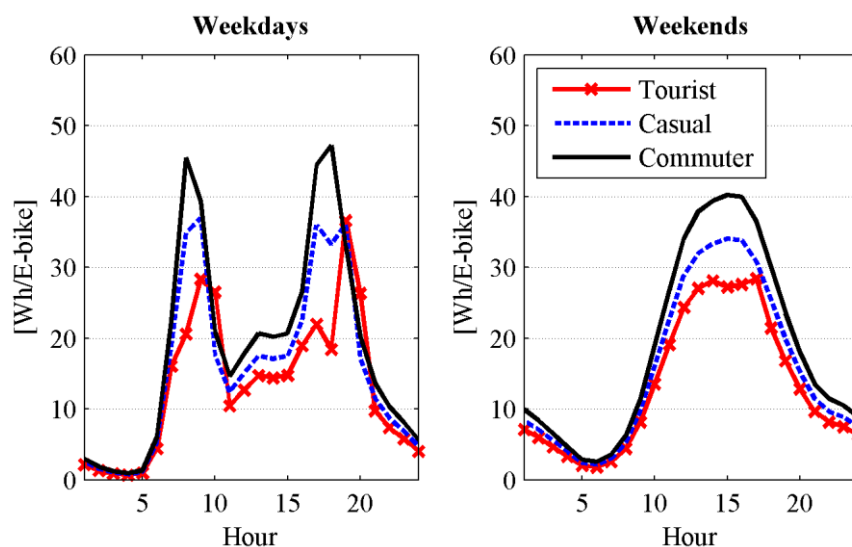


Figure 23. Average energy supplied from the power supply per E-bike during weekdays and weekends during high usage at 10.8 trips/(hour & day).

Figure 23 shows the average energy supplied from the power supply per E-bike during weekdays and weekends. What can be noted is that most of the charge energy supplied is during daytime since the E-bikes are most used then. The implication from this is that the energy needed for charging matches quite well with the solar irradiation (see Figure 2).

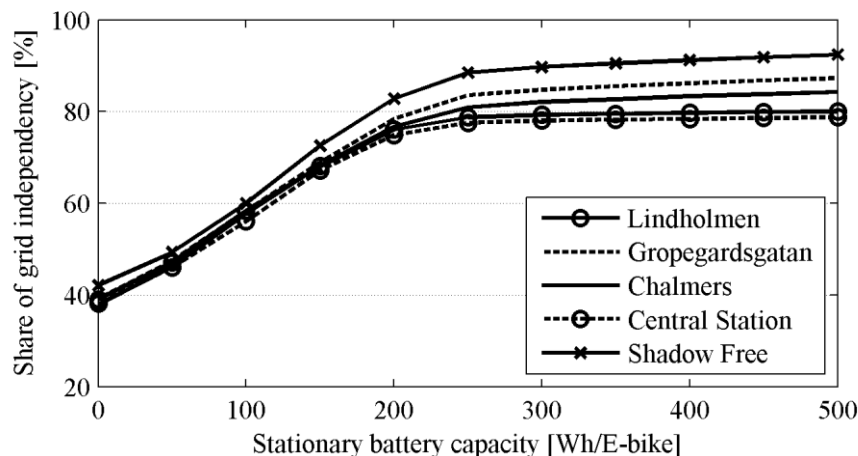


Figure 24. Share of the time there is no energy flow from the grid dependent on the size of the stationary battery. The rider profile used in all cases were commuter and the solar panel area was set to  $2 \text{ m}^2$  and the assumed use 10.8 trips/(bike & day).

By introducing a stationary battery to a grid-connected system, it is possible to reduce the power flow from the grid, see Figure 24. (Further examples are presented in Appendix 5 for other solar panel areas.) This result can be useful if the system should be designed to operate as much as possible without power exchange with the grid. An application of such a system can be to inform the users when their ride is 100% powered by the sun. In Figure 24 it can be seen that the grid independency flattens out for larger stationary battery capacities. (More graphs are shown in Appendix 5 for various system options.) This is due to that the electrical energy from the solar panels is limited. To reach higher grid independency it is thus better to consider larger panel area instead of more batteries. This is also good from a resource perspective since the panels actually generate electrical energy whereas the batteries just act as a buffer.

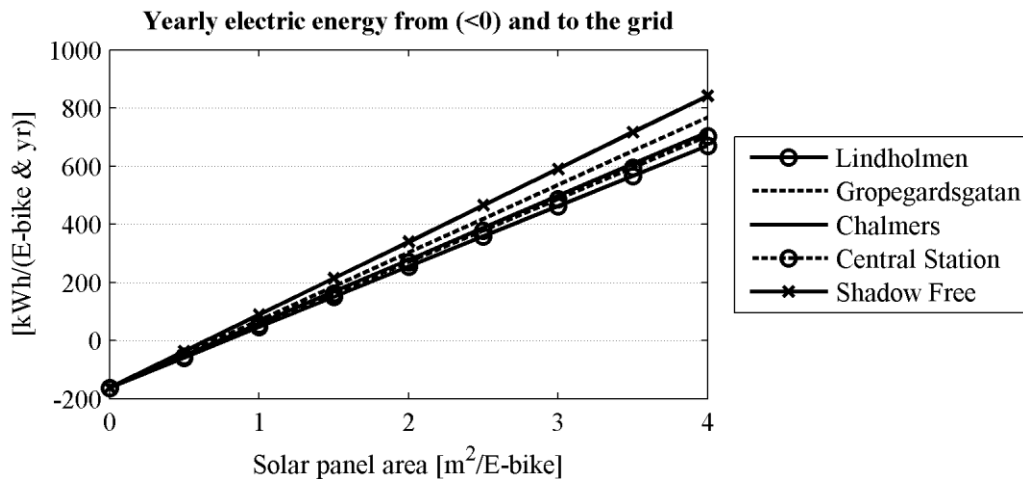


Figure 25. Yearly electric energy from (<0) and to the grid depending on solar panel area. Energy use was computed for the commuter profile at an assumed use of 10.8 trips/(bike & day).

The solar panel area needed to supply the yearly energy demand from the simulated E-BSS is around  $0.8 \text{ m}^2/\text{E-bike}$  for the studied locations at high system usage at 10.8 trips/(bike & day) (see Figure 25). If the use is decreased to 3 trips/(bike & day), which is the use in London's BSS, the solar panel area needed for yearly energy self-sufficiency is  $0.2\text{-}0.3 \text{ m}^2/\text{E-bike}$  (see Appendix 6 for graphs with 3, 5 and 10.8 trips/(bike and day)). The computed solar panel area is well below the assumed maximum area at  $3\text{-}3.8 \text{ m}^2/\text{E-bike}$  (see Table 5). If the solar panel area is larger than  $0.8 \text{ m}^2/\text{E-bike}$  for the system in Figure 25 it will be a net generator of electrical energy. The yearly amount of energy fed to the grid is shown in Figure 25 for different solar panel areas. This is independent on stationary battery size as the average energy from a battery during a charge-discharge cycle is ideally zero.

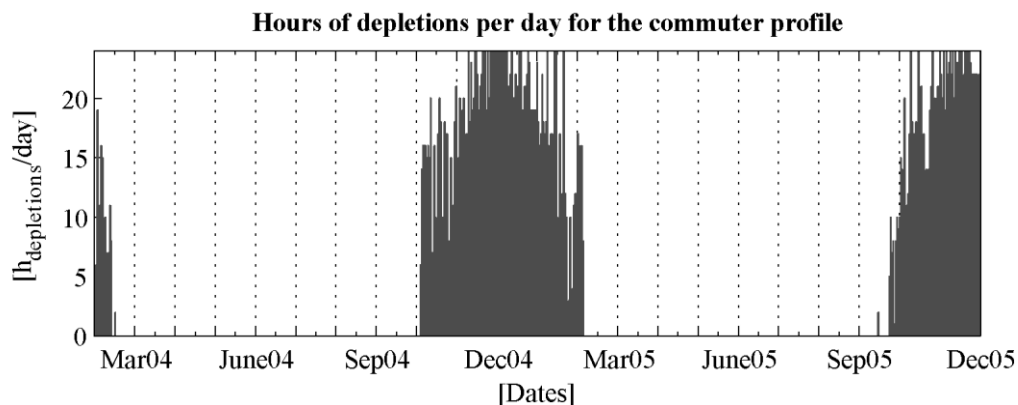


Figure 26. Hours of depletions per day for an off-grid system without any buffer battery. Simulation is performed for a solar panel area at  $2 \text{ m}^2$ , the commuter profile and high system use at 10.8 trips/(bike & day).

If the E-BSS is off-grid, careful consideration is needed in the design process to ensure that the energy supplied by the solar panels is enough for the demand. Figure 26 shows the average hours of E-bike battery depletions per day for an off-grid system without any buffer battery (more examples are shown in Appendix 7). Including a buffer battery would

essentially smooth the curve out but it cannot make the system function during e.g. December as it does not supply any energy to the system, it just acts as a buffer. The system shown in Figure 26 could perhaps be operating without major disturbances from mid April to the end of August if a buffer battery of sufficient size would be introduced. To enable full-year operation however, the solar panel area would have to be increased. A drawback with this compared to the on-grid case is that the system efficiency will be low as a lot of solar energy summertime will be unused.

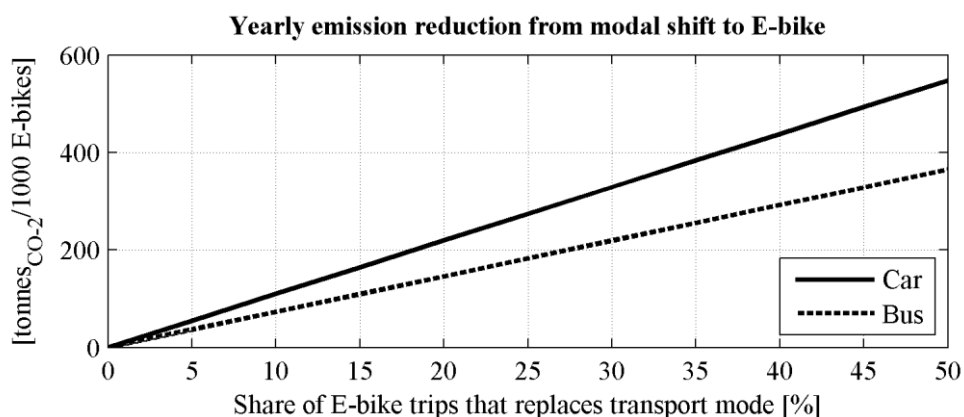


Figure 27. Yearly emission savings when introducing a system of 1000 E-bikes depending on the share of trips replaced by either car or bus. Assumptions: 5 trips/(E-bike & day), 5 km average trip distance; emissions: 120 gCO<sub>2</sub>/passengerkm for a gasoline car and 80 gCO<sub>2</sub>/passengerkm for a diesel city bus (Göteborgs Stad, 2011); and 2 m<sup>2</sup> solar panel area/E-bike.

Figure 27 shows the yearly emission reductions when introducing an E-BSS on large scale and replacing trips with either gasoline car or diesel city bus. It is assumed that the system is grid-connected and consists of 1000 E-bikes which is a similar size as Gothenburg's current BSS. The total reduction would thus be the sum of the respective modal shift. If for example 30% of the trips replaces bus and 10% replaces car, about 300 tonnes CO<sub>2</sub>/1000 E-bikes would be reduced annually. In addition to that, around 300 MWh/year of solar energy would be fed into the grid. The emission savings would be lower in the future as busses and cars are getting more efficient each year. The amount of energy fed to the grid would however be the same.

## 7. Discussion

E-bikes are more than thirty times as energy efficient as cars (see Figure 29). As a transport mode they have great potential to decrease emissions and congestion. They enable ride in high speed despite strong headwind or hilly conditions where regular cyclists would decrease their speed significantly. Due to the decreased human force needed for propulsion, longer rides are also easier making it an alternative to replace for example



car commuting. Combining E-bikes with bike pools also opens up their use to a broader audience as the initial cost decreases. The lack of ownership also means that the users do not have to worry

Figure 28. Area covered by 10 min on E-bike (20 km/h) and walking (5 km/h.)

about getting their E-bike stolen or to pay for maintenance. E-bikes can also be a natural extension to public transport. For commuters there might be a reduction in walking and waiting time to or between public transport station. E-bike stations would also increase the transport network size. Say that an E-bike station is placed at a bus station; the area covered by 10 minutes of E-bike ride from that spot is about fifteen times as large as if the person would walk as seen in Figure 28. Another benefit with E-bike station is that they can be placed more closely to where people start and end their journeys, such as homes or workplaces, than what is possible with for example tram and bus stations.

### 7.1 Weaknesses and uncertainties

This report is an exploratory study and hence contains a lot of assumptions that vary with system design, location, etc. It should thus be noted that results might vary significantly from a real-life E-bike pool. It has been tried throughout the calculations to have a good safe margin to ensure that the drawn conclusions are valid even though the system has high usage and long travel distances. In addition uncertain design parameters, there are a number of other uncertainties that may have affected the results. The used solar irradiation data is from two years only and is thus not representative of the long-term average irradiation. There is also an uncertainty in the irradiation data itself, especially as Sweden is located in the edge of the satellite's field of view. The data uncertainty is in the range of  $\pm 10\%$ . Furthermore, there is an uncertainty introduced due to the interpolation of irradiation during some of the winter months. However, as the irradiation is low during that period, even though the uncertainty might be high, the effect on yearly energy yield is low. The total energy use during an E-bike trip is dependent on the rider's weight, the route chosen and the wind. These will in turn be dependent on station locations and pricing which means that the reality of an E-BSS will look different than the computed results.

A factor that has not been accounted for in the calculations is that the usage of the E-bikes will vary with season and weather. It is likely that the use will be higher during summertime than wintertime and that more people will use the bikes when

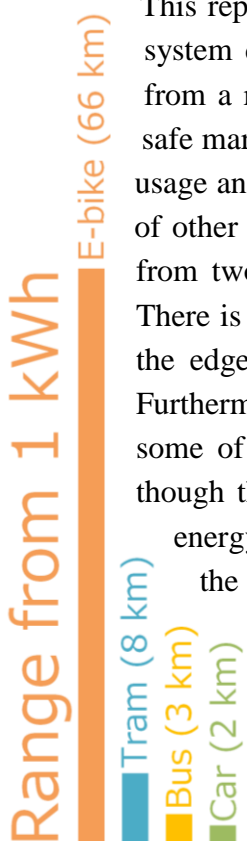


Figure 29. Range from 1 kWh of energy. E-bike: 15 Wh/km (incl. human energy) and the other transport modes from Göteborgs Stad (2011).

the weather is good. These user characteristics follows the solar irradiation well which could lead to higher grid independency than presented in this report.

One assumption made during the calculations is that battery charging is possible at all time. This will only be the case if battery heating of some sorts is implemented. It is also assumed that the charging power is constant during the charging cycle which is not the case for an actual Li-ion battery. The power electronics is assumed to have a MPPT function built in, this is usually incorporated in grid-tie inverters but not in all charge controllers for off-grid applications.

There are also two parts of the E-BSS that has been excluded in the calculations; the energy use by the locks and the terminal. Locking can however be made energy efficient so that power only is needed during the movement of the lock. The terminal has been excluded as it may be designed in very various ways. From a low-power computer without monitor that lets the user check out a bike via a phone application to a large monitor with a full-size computer. If an E-BSS is being designed and the terminal and locking energy use is known it is however easy to include. A rule-of-thumb for Gothenburg is that one square meter of solar panel can supply about 23 W of power as the yearly average. As stated earlier, this report is exploratory and contains many assumptions. However, due to the sensitivity analysis made the results are likely to be valid even though many parameters would change in reality.

## **7.2 The energy system**

What has been shown is that placing solar panels on the stations' roofs can result in net electric energy production from the stations to the grid with relatively small panel areas (0.2-0.8 m<sup>2</sup>/E-bike). A modal shift from for example car commuting or bus would therefore not only decrease the energy use and emissions, but potentially also lead to net generation of electricity. If for example an E-BSS would be built in Gothenburg with the same size as the current BSS, that could potentially save several hundred tonnes of CO<sub>2</sub> annually if the E-bike trips replaces some fossil fuel powered transport modes (see Figure 27). In addition to that, a couple hundred MWh of solar energy would be fed to the grid.

Choosing to build an off-grid solution can be useful in some cases such as temporary installations but is not seen as a viable large-scale system design. This is due to the fact that for an off-grid system to be operating over a long period of time, it must be designed to function the days with the lowest solar irradiation. The excess energy during days of high solar irradiation is thus not utilised. Using an on-grid solution with solar panels and a buffer battery seem as the best design. First and foremost, it makes it possible to design a system where the grid energy exchange is minimised while still enable excess solar energy production to be fed to the grid. A counter-argument towards placing solar panels in urban environment is that more energy would be generated by placing them on a shadow-free surface such as a rooftop nearby. Although that is true, a large share of the energy is still

available and several factors make it beneficial to keep the panels on the stations' roofs. First and foremost, it enables origin marking of electricity and increased system efficiency, as the electricity does not need to be converted to Alternating Current (AC) as often as an on-grid system without a buffer battery would. A second reason is that if an E-bike station is going to be built; placing a roof with solar panels over the docking spaces will not affect the area used. Placing the solar panels elsewhere would thus mean that more area is needed. It might also not be economically feasible to pay for a second piece of land. Lastly, placing solar panels in an urban environment means that it is exposed to a lot of people every day. This is an opportunity that can be seized and used to educate people on solar energy and energy systems. Monitors could be set up showing for example the instantaneous power and power balance or the daily energy yield. Another educational strategy could be to produce education material towards school classes that can use online data to do labs.

In order to get as low amount of battery depletions as possible, a simple charging strategy could be implemented. When a user wants to check out an E-bike, the bike with the most charge is unlocked. To ensure that the user has sufficient charge for a ride — and that the battery is well maintained — there could also be a lower value of the battery level set where the E-bike is kept locked until it has sufficient charge. Another method to decrease the occurrences of depletions is to increase the charging current. In this report, 2 A was used but in reality it could be increased to e.g. 5 A. A problem regarding battery charging arises in cold temperatures as Li-ion batteries should not be charged when the temperature is getting close to zero degrees. One solution is to keep the batteries in a heated cabinet at the station. This would not only allow safe charge during cold temperatures but could also supply fully charged batteries at all times if there are more batteries than E-bikes in the system. It has been shown however that battery depletion on a grid-connected system without battery swapping is likely not a problem despite high use (10.8 trips/(E-bike & day)). The need for a battery cabinet is thus not seen necessary from that perspective. A drawback with the cabinet solution is that the user must remember to take out the battery and mount it onto the E-bike and then vice versa on each ride. An alternative solution to charging cold batteries is to have a heating blanket built in the battery casing that would heat the battery using electric energy. The charging would then start when the battery is warm enough. Both solutions require extra input of energy that has not been accounted for in the calculations in this report. The need for battery heating is also dependent on the chosen season the pool should be operating. For full year operation it was shown that heating will be needed approximately 30% of the time (see Figure 20).

### **7.3 The operational perspective**

The economic perspectives of E-BSS have not been studied in this report. E-bikes for pool purposes are not currently mass-produced. A part of the investment cost of an E-BSS will thus go to development and the cost thus increases relative regular BSS. Of course it is possible to use off-the-shelf E-bikes and convert them for pool use. Using common E-bikes could

however lead to increased vandalism and theft. If no operator is willing to take the investment and operation cost themselves, further research should be made on business models on solar powered E-bike pools. It should be noted that it is possible to get revenue from the excess solar energy by selling it to electricity trading companies. The revenue from this is however low compared to the total system cost as one kWh fed to the grid gives about 1 SEK. That means that the revenue would be between 300-800 SEK per E-bike and year at 2-3.8 m<sup>2</sup> solar panel per E-bike.

One aspect that should be discussed thoroughly before setting up an E-BSS is safety. Users may not have driver's licence and may thus not know basic traffic regulations needed to ride safely in city centres with busses, trams, cars and pedestrians around. This is obviously already the case for regular BSS, but with higher speeds and accelerations, the risk of accidents increases. Another issue is helmets. It is unlikely that all users that would like to wear helmets when riding are willing to carry their own around. Some kind of helmet sharing or foldable helmet for sale could thus be considered. The possibility to ride in high speed with E-bikes (up to 25 km/h with electric drive) is possibly an issue. Depending on user behaviour, it might be necessary to limit the speed as 25 km/h is too high speed on for example a crowded, shared bicycle and pedestrian lane.

As users of regular BSS more often use their bike downhill than uphill, redistribution uphill is needed. A topic of future research can thus be to see if, and by how much, E-bike pools can decrease the need for redistribution relative regular BSS.

If an E-BSS is built it is recommended to publish data as open and detailed as possible. It gives others the opportunity to perform research or business around the E-bike pools. The trip distribution profiles in this report have for example been computed from open data published by Transport for London.

The stations could also serve as public charging poles for private E-bikes. As there are many charging connectors on the market there is probably need for supplying a wide range of connectors to ensure that they may be used. The stations could also include several types of electric vehicles. This could be E-bikes with children seats, electric cargo-bikes or bicycle trailers that can be connected to the E-bikes. A wider range of vehicle types could encourage a wider use such as trips to the food store or to leave children at kindergarten.

## 8. Conclusions

From a future energy system perspective, it is important to identify new ways of transport and generation of electricity and solar powered E-bike pools may just be such a case. E-bikes are an order of magnitude more energy efficient than car, bus or other heavy transport mode. Using a solar panel at 0.2-0.8 m<sup>2</sup> per E-bike has been shown to be enough to supply the early energy demand by the E-bike pool depending on simulated system usage (3-10.8 trips/(bike & day)). The computed area is smaller than the assumed maximum area at 3-3.8 m<sup>2</sup>/E-bike meaning that energy self-sufficiency on a yearly scale can be accomplished without running out of space. Using larger panel area than 0.2-0.8 m<sup>2</sup> per E-bike will for a grid-connected system lead to net electric energy production. A modal shift from bus or car to solar powered E-bike pool would thus not only reduce emissions and energy use but can potentially also lead to net production of electricity from solar energy.

The recommended system design is to have a grid-connected system as an off-grid solution would not utilise the solar irradiation fully. Coupling the grid-connected system with a buffer battery was shown to increase the share of time the system is independent of energy from the grid from about 40% to 80% at 2 m<sup>2</sup> solar panels per E-bike. The main benefit of introducing a buffer battery is that it enables origin marking of the electricity when the grid has not been used and that the system efficiency increases as less energy from the solar panel is converted to AC. Such origin marking can be used to inform the user that their E-bike now is powered 100% by solar energy. Having a system that is operating during a shorter period of the year would increase the grid independency as it is during wintertime the grid is needed the most due to the low solar irradiation. It was shown that the effect of the buffer battery flattens with increasing battery capacity. Increasing the grid-independency when this plateau has been reached can therefore be obtained by increasing the solar panel area.

It was shown that battery depletions are unlikely for on-grid systems despite high use of the E-bikes. The battery size could therefore be lowered if the use is known in more detail which would reduce the E-bike cost. A prerequisite for the results on depletion is that the battery level of an E-bike is tried to be averaged by letting the E-bike with the most charge to go at check-out. A further method of decreasing the risk of battery depletions is to increase the charging current. Increasing the charging current reduces the battery lifetime so unless there are problems with a certain level there is no reason to increase it. Battery heating of some sorts will be necessary if the system should be operating during cold periods (<5°C).

## 9. References

- Alonso García, M. & Balenzategui, J., 2004. Estimation of photovoltaic module yearly temperature and performance based on Nominal Operation Cell Temperature. *Renewable Energy*, Volume 29, pp. 1997-2010.
- Arrhenius, S., 1896. On the Influence of Carbonic Acid in the Air upon the Temperature of the Ground. *Philosophical Magazine and Journal of Science*, pp. 237-276.
- Atkinson, D., 2012. *2013 e-Bikes roundup - hub motors, shaft drives and more....* [Online] Available at: <http://road.cc/content/news/66564-eurobike-2012-e-bikes-roundup> [Accessed 24 February 2014].
- Badescu, V., 2002. 3D isotropic approximation for solar diffuse irradiance on tilted surfaces. *Renewable energy*, Volume 26, pp. 221-233.
- Bolton, O. J., 1895. *Electrical Bicycle*. U.S., Patent No. 552271.
- Bosch, 2014. *Bosch eBike Systems*. [Online] Available at: [http://www.bosch-ebike.de/en/produkte\\_neu/intuvia\\_1/intuvia\\_2.php](http://www.bosch-ebike.de/en/produkte_neu/intuvia_1/intuvia_2.php) [Accessed 27 March 2014].
- Breyer, C. & Schmid, J., 2010. *Population Density and Area Weighted Solar Irradiation: Global Overview on Solar Resource Conditions for Fixed Tilted, 1-Axis and 2-Axes PV Systems*, Sonnenallee, Germany: Q-Cells SE.
- Cadex, 2014. *Charging at High and Low Temperatures*. [Online] Available at: [http://batteryuniversity.com/learn/article/charging\\_at\\_high\\_and\\_low\\_temperatures](http://batteryuniversity.com/learn/article/charging_at_high_and_low_temperatures) [Accessed 8 May 2014].
- de Hartog, J. J., Boogaard, H. & Hoek, G., 2010. Do the Health Benefits of Cycling Outweigh the Risks?. *Environmental Health Perspectives*, 118(8), pp. 1109-1116.
- Dimroth, F., 2013. *Press Releases 2013: World Record Solar Cell with 44.7% Efficiency*. [Online] Available at: <http://www.ise.fraunhofer.de/en/press-and-media/press-releases/presseinformationen-2013/world-record-solar-cell-with-44.7-efficiency> [Accessed 27 January 2014].
- EcoRide, 2014. *EcoRide*. [Online] Available at: <http://www.ecoride.se/> [Accessed 24 February 2014].
- Electricbike.com, 2013. *Torque Sensors on Electric Bikes*. [Online] Available at: <http://www.electricbike.com/torque-sensors/> [Accessed 27 March 2014].
- Energimyndigheten, 2014. *Fortsatt starkt intresse för solceller gav solcellseffekt på 43,1 MW under 2013*. [Online] Available at: <http://www.energimyndigheten.se/Press/Pressmeddelanden/Fortsatt-starkt-intresse-for-solceller-gav-solcellseffekt-pa-431-MW-under-2013/> [Accessed 13 March 2014].
- Gladdis, K., 2013. London's 4.000 Boris bikes cost taxpayers €1,400 for each bicycle every year despite sponsorship from Barclays. *Dailymail*, 11 July.

- Green, M. A. et al., 2013. Solar cell efficiency tables (version 43). *Progress in Photovoltaics: Research and Applications*, Volume 22, pp. 1-9.
- Gulin, M., Vasak, M. & Baotic, M., 2013. *Estimation of the global solar irradiance on tilted surfaces*. Dubrovnik, Croatia, 17th International Conference on Electrical Drives and Power Electronics.
- Göteborgs Stad, 2011. *Spara energi - en utaning i Göteborgs stadsdelar*, Göteborg: Göteborgs Stad.
- IEA, 2011. *Solar Energy Perspectives*, Paris: International Energy Agency.
- IPCC, 2007. *Technical Summary — Climate Change 2007: Mitigation. Contribution of Working Group III to the Fourth Assessment Report of the Intergovernmental Panel on Climate Change*, Cambridge, UK and New York, NY, USA: Cambridge University Press.
- ITDP, 2013. *The Bike-share Planning Guide*, New York City: Institute for Transportation & Development Policy.
- Jakhrani, A. Q., Othman, A. K., Rigit, A. R. & Samo, S. R., 2011. Comparison of Solar Photovoltaic Module Temperature Models. *World Applied Sciences Journal*, 14(Special Issue of Food and Environment), pp. 1-8.
- JCDecaux, 2014. *Styr & Ställ Göteborg*. [Online]  
Available at: <http://www.goteborgbikes.se/>  
[Accessed 5 March 2014].
- King, D. L., Kratochvil, J. A. & Boyson, W. E., 1997. *Measuring Solar Spectral and Angle-of-Incidence Effects on Photovoltaic Modules and Solar Irradiance Sensors*, Albuquerque: Sandia National Laboratories.
- Konsumentverket, 2012. *Nybilsguiden - Om bränsleförbrukning och vår miljö*, Karlstad: Konsumentverket.
- Kopp, G. & Lean, J. L., 2011. A new, lower value of total solar irradiance: Evidence and climate significance. *Geophysical Research Letters*, 38(1).
- Langford, B. C. et al., 2013. North America's First E-Bikeshare: A Year of Experience. *Transportation Research Record: Journal of the Transportation Research Board*, Volume 2387, pp. 120-128.
- Lifebike, 2014. [Online]  
Available at: <http://www.lifebike.se/>  
[Accessed 26 February 2014].
- Malamut, M., 2014. 'Prescribe-a-bike' Coming To a Hospital Near You. *Boston Magazine*, 26 March.
- Martin, N. & Ruiz, J. M., 2001. Calculation of the PV modules angular losses under field conditions by means of an analytical model. *Solar Energy Materials & Solar Cells*, Volume 70, pp. 25-38.
- Matzarakis, A. & Matuschek, O., 2011. Sky view factor as a parameter in applied climatology — rapid estimation by the SkyHelios model. *Meteorologische Zeitschrift*, 20(1), pp. 39-45.
- Morchin, W. C., 1996. *Trip Modeling for Electric-Powered Bicycles*. Seattle, WA, IEEE Technical Applications Conference, Northcon 95, pp. 373-377.

- Morchin, W. & Oman, H., 2006. *Electric Bicycles: A guide to Design and Use*. New Jersey, NY, U.S.: IEEE Press.
- Muetze, A. & Tan, Y. C., 2007. Electric Bicycles - A performance evaluation. *IEEE Industry Applications Magazine*, July, August.
- MyEco, 2014. *Våra Cyklar*. [Online]  
Available at: <http://www.myeco.se/>  
[Accessed 26 February 2014].
- NASA, 2014. *NASA Surface meteorology and Solar Energy - Location*. [Online]  
Available at: <https://eosweb.larc.nasa.gov/cgi-bin/sse/grid.cgi?email=skip@larc.nasa.gov>  
[Accessed 23 January 2014].
- Navigant Research, 2014. *Electrical Bicycles*. [Online]  
Available at: <http://www.navigantresearch.com/research/electric-bicycles>  
[Accessed 22 January].
- NREL, 2011. *How to Interpret PVWatts Results*. [Online]  
Available at: [http://www.nrel.gov/rredc/pvwatts/interpreting\\_results.html](http://www.nrel.gov/rredc/pvwatts/interpreting_results.html)  
[Accessed 22 January 2014].
- OBIS, 2011. *Optimising Bike Sharing in European Cities - A Handbook*. [Online]  
Available at: <http://www.obisproject.com/>
- Oja, P. et al., 2001. Health benefits of cycling: a systematic review. *Scandinavian Journal of Medicine & Science in Sports*, 21(August), pp. 496-509.
- Panasonic, 2014. *HIT photovoltaic module HIT-N245*, Munich: Panasonic.
- Panasonic, 2014. *Lithium-Ion, Technical Data*. [Online]  
Available at: <http://www.panasonic.com/industrial/batteries-oem/oem/lithium-ion.aspx>  
[Accessed 24 February 2014].
- Pompermaier, C., Sjöberg, L. & Nord, G., 2012. *Design and optimization of a Permanent Magnet Transverse Flux Machine*, Höganäs: Höganäs.
- Poortmans, J. & Arkhipov, V., 2006. *Thin Film Solar Cells: Fabrication, Characterization and Applications*. New York: John Wiley & Sons.
- Prampero, P. E. d., 2000. Cycling on Earth, in space, on the moon. *European Journal of Applied Physiology*, Volume 82, pp. 345-360.
- Rauschenbach, H. S., 1980. *Solar Cell Array Design Handbook: The Principles and Technology of Photovoltaic Energy Conversion*. New York: Van Nostrand Reinhold Company.
- Reda, I. & Andreas, A., 2008. *Solar Position Algorithm for Solar Radiation Applications*, Colorado: National Renewable Energy Laboratory (NREL).
- Reich, N. H. et al., 2005. *Weak Light Performance and Spectral Response of Different Solar Cell Types*. Barcelona, Proceedings of the 20th European Photovoltaic Solar Energy Conference and Exhibition.
- Rojas-Rueda, D., de Nazelle, A., Tainio, M. & Nieuwenhuijsen, M. J., 2011. The health risks and benefits of cycling in urban environments compared with car use: health impact assessment study. *BMJ*, 4 August.

- Roy, J. V. et al., 2011. *An Availability Analysis and Energy Consumption Model for a Flemish Fleet of Electric Vehicles*. Brussels, EEVC European Electric Vehicle Congress.
- Rubbee, 2014. *Rubbee*. [Online]  
Available at: <http://www.rubbee.co.uk/>  
[Accessed 24 February 2014].
- Sandén, B., 2013. *Systems Perspectives on Electromobility*, Gothenburg: Chalmers University of Technology.
- Sandqvist, W., 2014. *Borstlösa PM-motorer*. [Online]  
Available at: <http://www.ict.kth.se/courses/IL1390/pmsm/index.htm>  
[Accessed 26 February 2014].
- Skoplaki, E. & Palyvos, J. A., 2009. On the temperature dependence of photovoltaic module electrical performance: A review of efficiency/power correlations. *Solar Energy*, Volume 83, pp. 614-624.
- SMHI, 2014. *Klimatdata: Öppna data*. [Online]  
Available at: <http://www.smhi.se/>  
[Accessed 20 March 2014].
- SoDa, 2014. *Solar Energy Services for Professionals*. [Online]  
Available at: <http://www.soda-is-com/>  
[Accessed 22 January 2014].
- Spagnol, P. et al., 2012. *A full hybrid electric bike: how to increase human efficiency*. Fairmont Quenn Elizabeth, Montréal, Canada, 2012 American Control Conference.
- Starschich, E. & Muetze, A., 2007. *Comparison of the Performance of Different Geared Brushless-DC Motor Drives for Electric Bicycles*. Antalya, IEEE International Electric Machines & Drives Conference, pp. 140-147.
- Thomas, C., 2013. *Missing data HelioClim-3v4* [Interview] (10 February 2013).
- Trafikkontoret, 2012. *Cykelåret 2012 - En sammanfattning av årets cykelförbättringar*, Göteborg: Göteborgs Stad.
- Transport for London, 2014. *Open data users: Our feeds*. [Online]  
Available at: <http://www.tfl.gov.uk/info-for/open-data-users/our-feeds?intcmp=4064>  
[Accessed 31 March 2014].
- United States Department of Energy, 2010. *The History of Solar*. [Online]  
Available at: [http://www1.eere.energy.gov/solar/pdfs/solar\\_timeline.pdf](http://www1.eere.energy.gov/solar/pdfs/solar_timeline.pdf)  
[Accessed 27 January 2014].
- University of Tennessee-Knoxville, 2014. *cycleUshare: Research*. [Online]  
Available at: <http://www.cycleushare.com/>  
[Accessed 6 May 2014].
- Weier, J. & Cahalan, R., 2003. *Solar Radiation and Climate Experiment (SORCE)*. [Online]  
Available at: <http://earthobservatory.nasa.gov/Features/SORCE/>  
[Accessed 22 January 2014].
- Zirnheld, J. & Muffoletto, D., 2011. *Rechargeable power source for electric vehicles*, Buffalo: University .

## Appendix 1

Appendix 1 presents a simplified model of six different vehicle types' energy use seen from a lifecycle perspective (including fuel generation only). Table A1.1 presents the efficiencies for the different energy supply chains. Most of the data is from Table 5.4 in the report *Systems Perspectives on Electromobility* by Sandén et al. (2013). Table A1.2 shows the well to wheel, and the solar energy to wheel, energy use for six different vehicle types.

**Table A1.1. Efficiency table for a set of supply chains of energy in transport.<sup>a</sup>**

Energy supply chain	Efficiency				
	Solar energy conversion	Conversion to fuel/battery storage	Distribution	Well to tank	Solar energy to tank
Crude oil-refinery-fuel oil-power plant-electricity		0.40	0.95	0.38	
Crude-oil-refinery-gasoline		0.85	0.99	0.84	
Solar energy-farming-corn-bio refinery-ethanol	0.003	0.25	0.99	0.25	0.0074
Solar energy-solar cell-electricity	0.15	0.99	0.95	0.94	0.14
Solar energy-farming-food	0.03	0.13 <sup>b</sup>	0.99	0.13	0.004

<sup>a</sup> Data source, Table 5.4 from Sandén (2013).

<sup>b</sup> Assuming 0.5 of plant is edible and human efficiency from chemical energy to mechanical is 0.25 (Prampetro, 2000).

**Table A1.2. Energy use when looking at fuel production from a lifecycle perspective.**

Vehicle type	Powered by	Tank to wheel	Well to wheel	Solar to wheel
			Electricity from: fossil / solar (excl. human power)	(excl. human power)
		Wh/km	Wh/km	Wh/km
Gasoline car	Gasoline	520 <sup>b</sup>	620	
Ethanol car	E85 (85% ethanol, 15% gasoline)	510 <sup>c</sup>	1750	537 000
Battery electric car	Electricity	180 <sup>d</sup>	470 / 190	1 300
Electric scooter	Electricity	40 <sup>d</sup>	110 / 40	290
E-bike	Electricity & human power <sup>a</sup>	9.3 <sup>e</sup>	50 / 40 (20) / (10)	1 150 (50)
Bicycle	Human power	7.5 <sup>e</sup>	60 (0)	1 940 (0)

<sup>a</sup> Assuming 50 W constant human power.

<sup>b</sup> Assuming 5.5 l/100 km (city drive cycle) (Konsumentverket, 2012).

<sup>c</sup> Assuming 8 l/100 km (city drive cycle) (Konsumentverket, 2012).

<sup>d</sup> Data from Roy et al. (2011).

<sup>e</sup> E-bike: Mass of rider and E-bike 100 kg, constant speed at 20 km/h and electric system efficiency at 75%.

Regular bike: Mass of rider and bike 90 kg, constant speed at 15 km/h.

Other constants: Air density 1.2 kg/m<sup>3</sup>, A=0.5 m<sup>2</sup>, C<sub>r</sub>=1, R<sub>c</sub>=0.0071, C<sub>d</sub>=1 and slope=1%.

## Appendix 2

This appendix includes further information about solar energy calculations for the interested reader.

### A2-1. Equation to compute the angle of incidence

$$\alpha_i = \cos^{-1}[\cos(\alpha_{panel}) \cos(\theta_{zenith}) + \sin(\alpha_{panel}) \sin(\theta_{zenith}) \cos(\gamma_{sun} - \gamma_{panel})], \quad (A2-1.1)$$

where  $\alpha_i$  is the angle of incidence between the incoming light and the normal to the solar panel,  $\alpha_{panel}$  is the panel's tilt,  $\theta_{zenith}$  the sun's zenith angle and  $\gamma_{sun}$ ,  $\gamma_{panel}$  the azimuth angle of the sun and the panel respectively (King, et al., 1997). All angles are in degrees ( $^\circ$ ) and are illustrated in Figure 11. The angle of incidence can be used in calculations of reflective losses or to calculate the direct irradiance in tilted condition when the direct normal irradiance is known.

### A2-2. Effect on irradiance of tilted planes

When a surface is horizontal, it receives direct and diffuse irradiance. Let us define those as the Beam (direct) Horizontal Irradiance (BHI) and the Diffuse Horizontal Irradiance (DHI) respectively. The sum of those to can be noted the Global Horizontal Irradiance (GHI). If the surface is tilted, it will affect those components in different ways. The direct irradiance towards the tilted panel can be noted as the Beam (direct) Tilted Irradiance (BTI) and is calculated by a simple cosine function

$$BTI = BHI \cos(\alpha_i), \quad (A2-2.1)$$

where  $\alpha_i$  is the angle of incidence (see Figure 11) and BHI the direct irradiance towards a horizontal plane. Determining the diffuse irradiance is a bit trickier as the distribution of irradiance on the hemisphere is unknown. Depending on method, one may assume either isotropic or anisotropic conditions (Gulin, et al., 2013). Isotropic may be used for latitudes not too far from the equator. In Sweden however, the sun has a rather low angle relative horizon which causes more diffuse irradiance from the southern part of the hemisphere than the northern. One of many methods (Gulin, et al., 2013) to estimate the diffuse irradiance from the horizontal data was presented by Badescu (2002) as,

$$DTI = DHI \frac{3 + \cos[2(90^\circ - \alpha_{panel})]}{4}. \quad (A2-2.2)$$

DTI is the diffuse tilted irradiance and DHI the diffuse horizontal irradiance as a function of the panel tilt. Estimating the ground reflected irradiance can be done using similar equations but such methods are not useful in this report as they assume no shadowing which will not be the case in the urban environment.

### A2-3. Equations to calculate reflective losses

In a paper by Martin and Ruiz (2001) on reflective losses of PV systems, it was concluded that the average monthly loss in energy yield varied from a few percent to about 15%. The paper presents formulas that can be used to estimate the loss of diffuse and direct irradiance due to reflection of light on the panel's surface. The formula to calculate the factor of direct irradiance after reflection is,

$$F_{direct} = 1 - \frac{\exp(-\cos(\alpha_i)/a_r) - \exp(-1/a_r)}{1 - \exp(-1/a_r)}, \quad (A2-3.1)$$

where  $F_{direct}$  is factor of reflection loss of direct irradiance (one in no loss conditions),  $\alpha_i$  is the angle of incidence towards the panel ( $^\circ$ ) and  $a_r$  is a constant depending on solar panel layout and degree of dust (see Table A2-3.3). The equation for the factor of diffuse irradiance left after reflection is,

$$F_{diffuse} = 1 - \exp\left[-\frac{1}{a_r} \left( C_1 \left( \sin(\alpha_p) + \frac{180 - \alpha_p - \sin(\alpha_p)}{1 + \cos(\alpha_p)} \right) + C_2 \left( \sin(\alpha_p) + \frac{180 - \alpha_p - \sin(\alpha_p)}{1 + \cos(\alpha_p)} \right)^2 \right)\right], \quad (A2-3.2)$$

where  $\alpha_p$  is the tilt angle of the solar panel ( $0^\circ$  is horizontal) and  $C_1$  and  $C_2$  are fitting parameters. The values of  $a_r$ ,  $C_1$  and  $C_2$  are presented in Table A2-3.3 for different solar panel technologies.

**Table A2-3.3. Fitting parameters for equations 5 and 6 depending on module type (Martin & Ruiz, 2001).**

Panel type	$a_r$	$C_1$	$C_2$
sc-Si	0.169	$4/(3\pi)$	-0.069
mc-Si	0.159	$4/(3\pi)$	-0.074
a-Si	0.163	$4/(3\pi)$	-0.074
Dusty Si panel	0.200	$4/(3\pi)$	-0.064

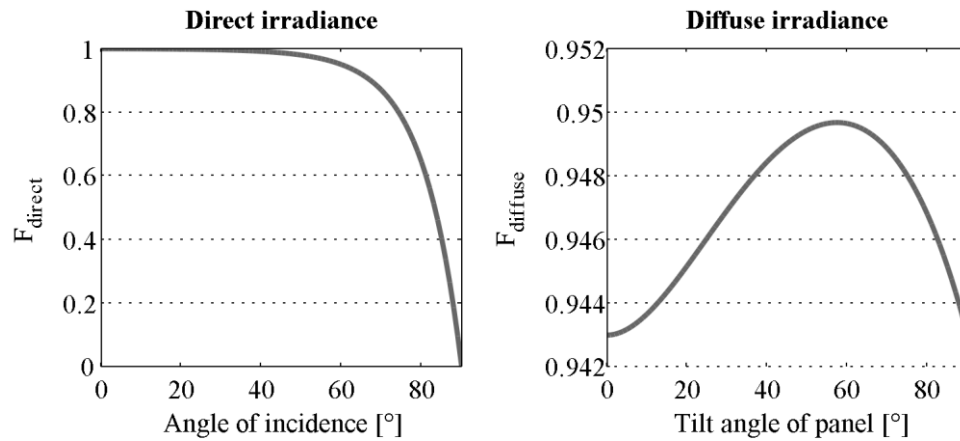


Figure A2-3.4. Factors for the irradiance components direct and diffuse due to reflection; one means no loss. Left: Factor for the direct irradiance as a function of angle between the direct irradiance and the normal to the solar panel. Right: Factor of the diffuse irradiance as a function of the panel's tilt angle ( $0^\circ$  being horizontal). Both for a sc-Si panel.

An example of how reflection affects the irradiance components depending on angle of incidence can be seen in Figure A2-3.4. In the left graph it can be noted that the loss of direct irradiance increases rapidly above  $60^\circ$  angle of incidence. The loss of diffuse irradiance due to reflection, seen in the right graph, is low compared to the loss of direct irradiance as over 94% of the diffuse irradiance is remaining in all cases.

#### A2-4. Sky view factor

An equation to compute the sky view factor was given by Matzarakis and Matuschek (2011),

$$\psi = 1 - \sum_{i=1}^n \sin^2(\beta_i) \left( \frac{\Delta\alpha_i}{360^\circ} \right), \quad (\text{A2-4.1})$$

where  $\psi$  is the sky view factor (i.e. the ratio between the area of the sky and the entire hemisphere),  $\beta$  the altitude angle and  $\Delta\alpha$  is the difference in azimuth angle between each sample. The input data to equation A2-4.1 originates from measurements on surrounding buildings at a specific location. The horizontal profiles measured for the locations presented in Table 4 can be seen in figure A2-4.2.

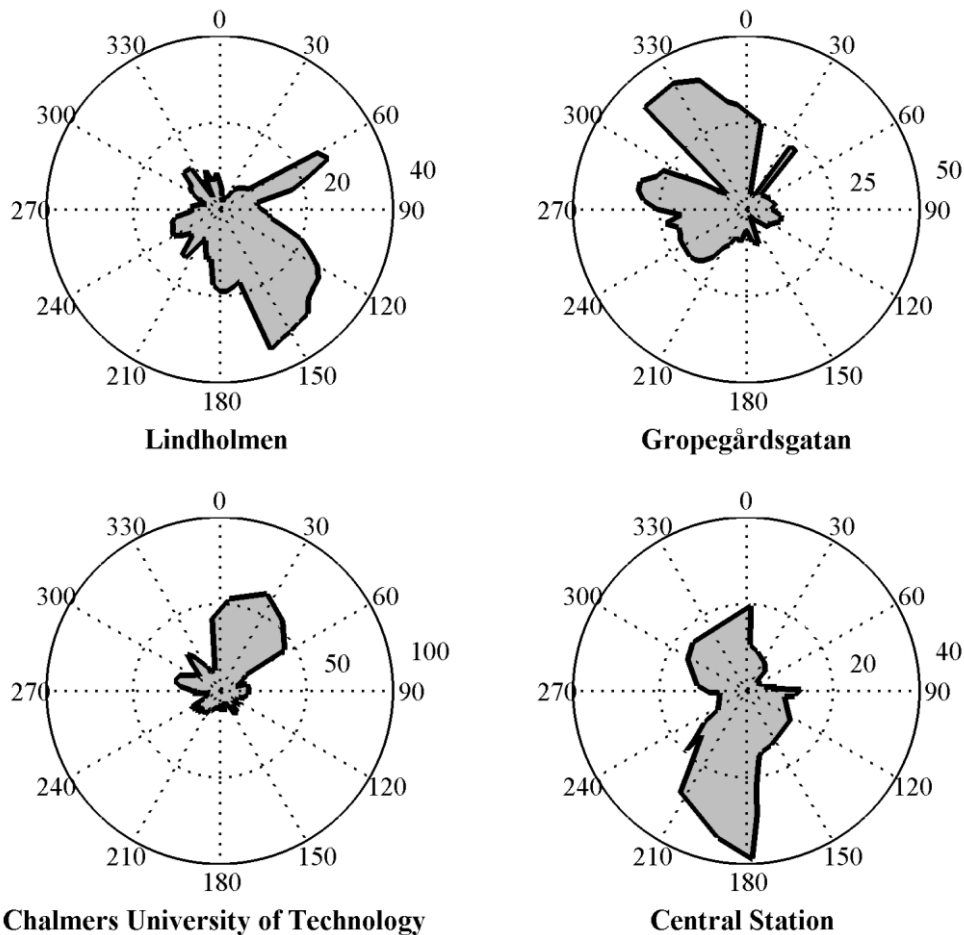


Figure A2-4.2. Horizontal profiles measured at the locations specified in Table 4. The figures around the circles marks the azimuth angles ( $^{\circ}$ ) and the radius from the centres the altitude angles ( $^{\circ}$ ).

### A2-5. Estimating the temperature of a solar panel

As the solar panel's efficiency decreases with increasing temperatures it is important to know the solar cell temperature. A common model that requires few input parameters is one discussed by García and Balenzategui (2004),

$$T_{cell} = T_a + (NOCT - 20) \frac{G}{800}, \quad (A2-5.1)$$

where  $T_a$  is the ambient temperature ( $^{\circ}\text{C}$ ),  $NOCT$  the temperature given in the module datasheet ( $^{\circ}\text{C}$ ) and  $G$  the irradiance ( $\text{W}/\text{m}^2$ ). A drawback with this method is that it only can be applied to freestanding modules that are not integrated in for example a roof or wall structure. There will also be a shift in the error of the model compared to the real cell temperature throughout a day due to accumulated heating in the afternoon (Alonso García & Balenzategui, 2004).

## Appendix 3

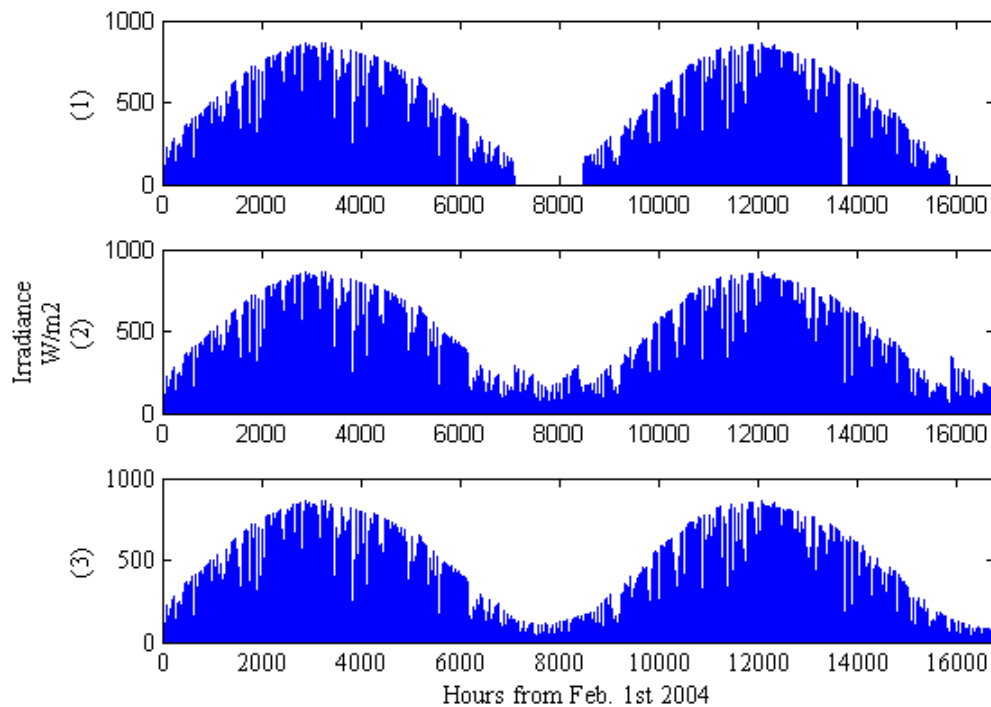


*Figure A3-1. Interpolation of data. (1) Example of original dataset where large spots of missing data can be seen around 8000 h and after 16000 h and two small spots can be noted around 6000 h and 14000 h. (2) First approximation; missing fields are filled by copying the surrounding data. (3) Result of the interpolation. The copied data is scaled according to a 11 degrees polynomial curve following the top of the curve.*

Due to the low solar angle during winter in Sweden, and a few errors in the HelioClim-3 irradiation data, there are gaps in the irradiation datasets; see the blank spots in Figure A3-1 (1). An interpolation methodology to fill these gaps was developed. The maximum possible irradiance on each day is dependent on the sun's position relative the solar panel. In A3-0 (1), it can be seen that the top of the curve follows a sinus function which in this case has a wavelength of one year. By analysing the maximum irradiance in periods of five days, a first estimation of the maximum irradiance curve could be established, see Figure A3-2.

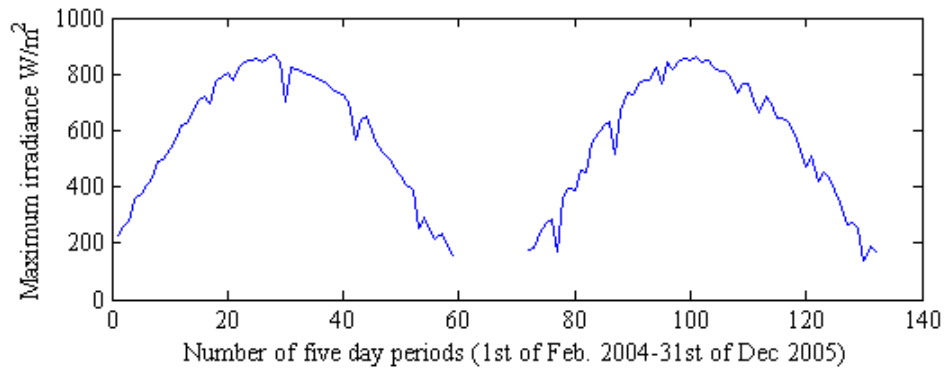


Figure A3-2. Maximum irradiance for periods of five days. (1 on the x-axis corresponds to 1st-5th of February, 2004 and 140, 27th-31st of December 2005.)

As a first approximation, the missing data was assumed to be equal to 0.5 times the mean of the two values before and after the gaps (see horizontal lines in A3-3). This initial estimation was performed for two reasons. First because the polynomial fitting curve cannot be used for incomplete datasets and secondly since introducing zeros would force the polynomial fitting curve too low. If there would be missing data in another period than the winter, the chosen constant would have to be changed. An automatic methodology could be developed that samples some points before and after the gap in order to estimate a trend. The constant 0.5 was chosen after trying different values for different irradiance datasets and observing the result in comparison to actual irradiance during winter with data from NASA (2014).

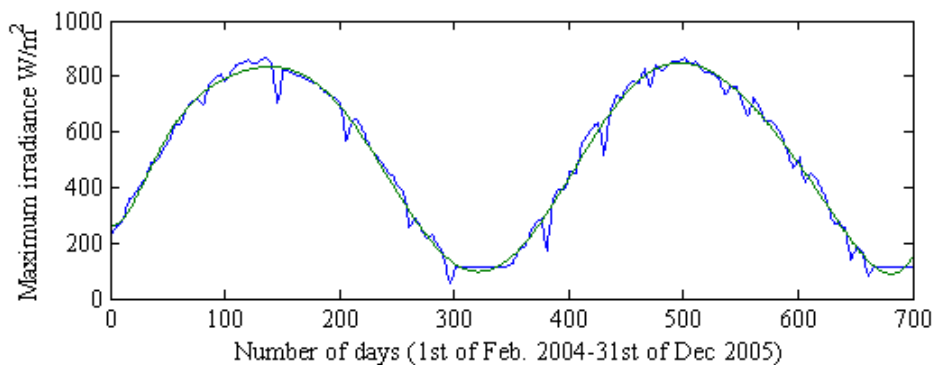


Figure A3-3. Maximum possible irradiance estimated for each day. Smooth line represents the fitting curve to the blue data.

It was shown that the error of the interpolated monthly irradiation was 15% above and 15% below the long-term averages from NASA for January and December respectively. That is still within the  $\pm 30\%$  range of monthly variation as described in section 4.1.1. After the missing data had been estimated, a polynomial fit of the 11th degree is applied, see the smooth line in Figure A3-3. The reason for the high number of degrees is that not all curves look like a simple sinus such as when a surface has high tilt (see Appendix A3-1). Having a lower amount of degrees means that these — more complex — curves cannot be followed.

Now when the maximum possible irradiance has been estimated as a polynomial function it is time to go back to the original dataset (Figure A3-1.1 (1)) to fill the gaps. At first, the missing data is filled by pure copying of the surrounding days as exemplified in Figure A3-1.1 (2). These days are then scaled to fit the polynomial function with the assumption that reaching the maximum irradiance level will happen once every fifth day. That is, the days with copied data is divided into five day long periods and for each period, the data is scaled with a factor that causes one irradiance point per period to reach the polynomial function. The same methodology is then used to interpolate all available datasets.

This section presents some examples of the result after interpolation of data. First graph in each figure (1), represents the raw data, (2) the data after surrounding data is copied and (3) shows the final result.

### A3-1. Further examples of irradiance data after interpolation

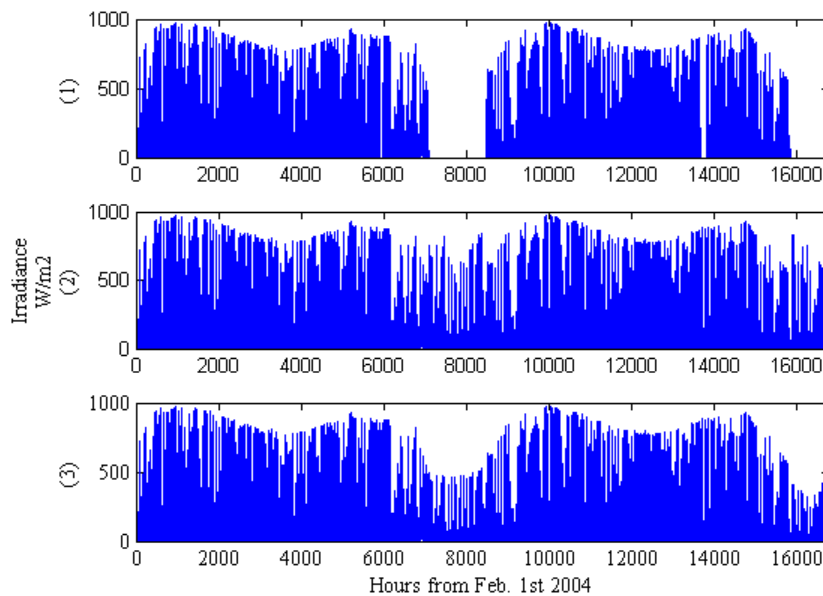


Figure A3-1.1. Irradiation interpolation in three steps for azimuth angle:  $180^\circ$ , Slope:  $80^\circ$ . (1) Is the original dataset, (2) after surrounding data has been copied and (3) the final result.

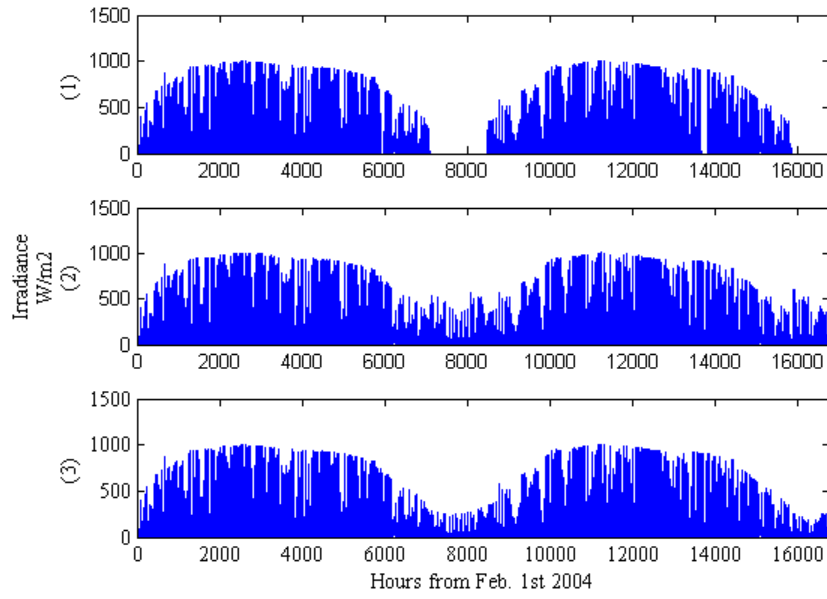
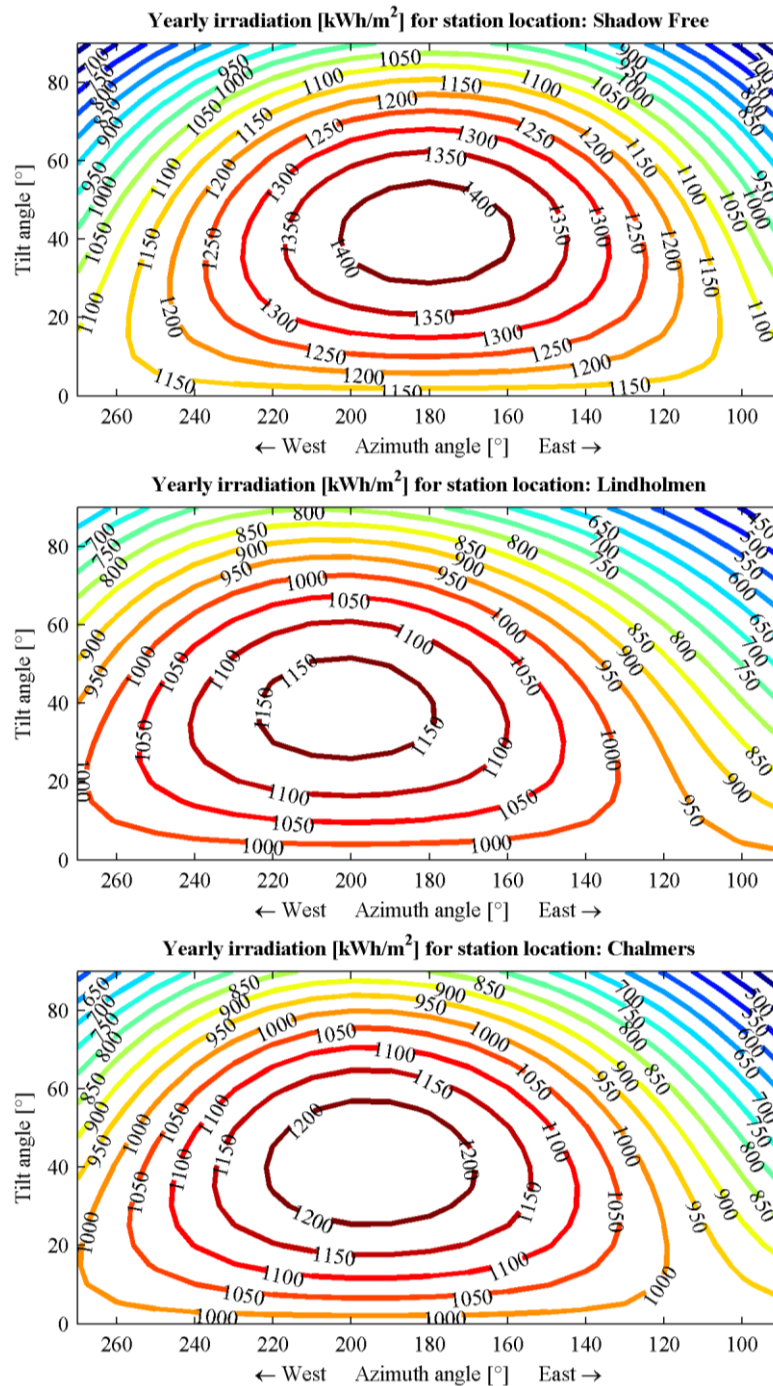


Figure A3-1.2. Irradiation interpolation in three steps for azimuth angle:  $110^\circ$ , Slope:  $65^\circ$ . (1) Is the original dataset, (2) after surrounding data has been copied and (3) the final result.

## Appendix 4

Contour plots of the yearly solar irradiation and electric energy yield for the studied locations depending on azimuth and tilt angle.

Figure A4-1. Contour plots of the yearly irradiation for the studied station locations depending on azimuth and tilt angle.



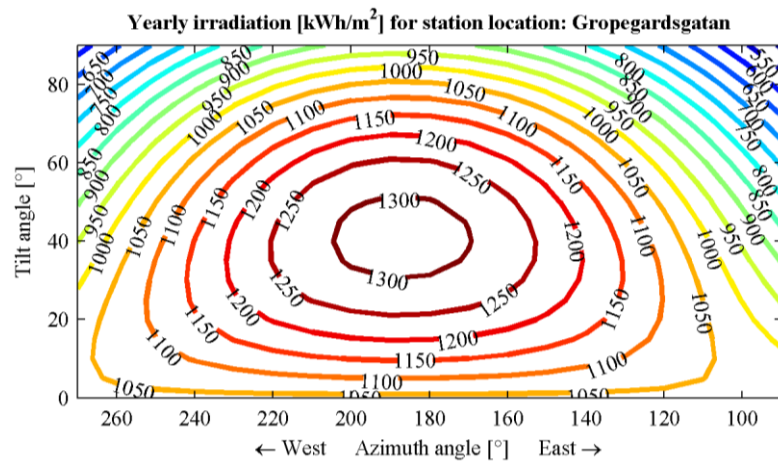
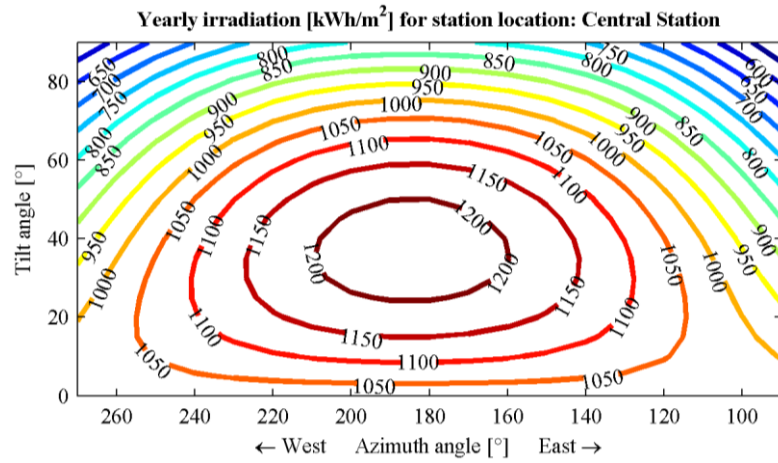
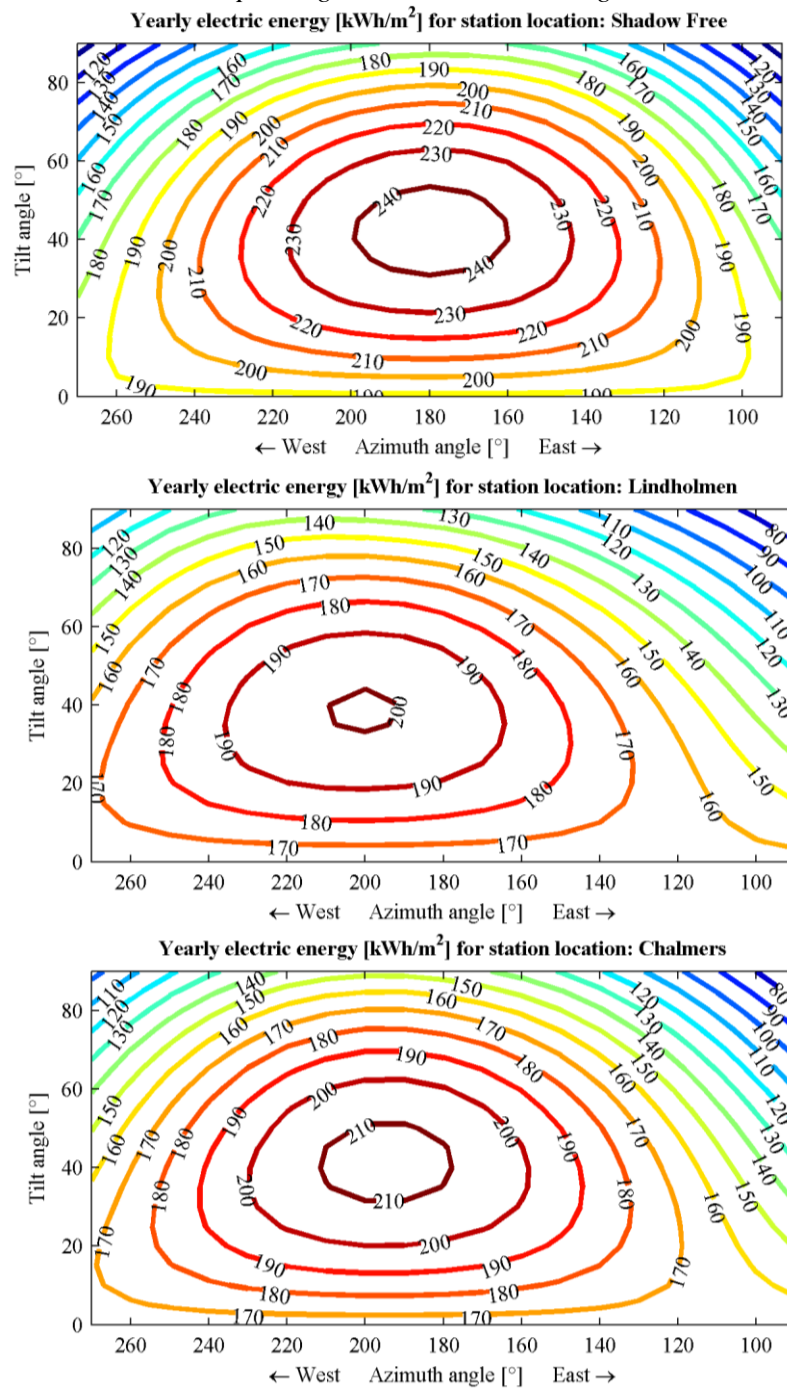
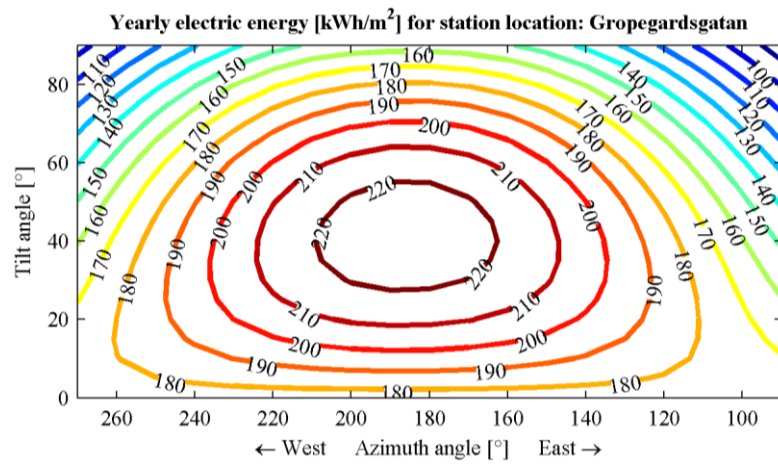
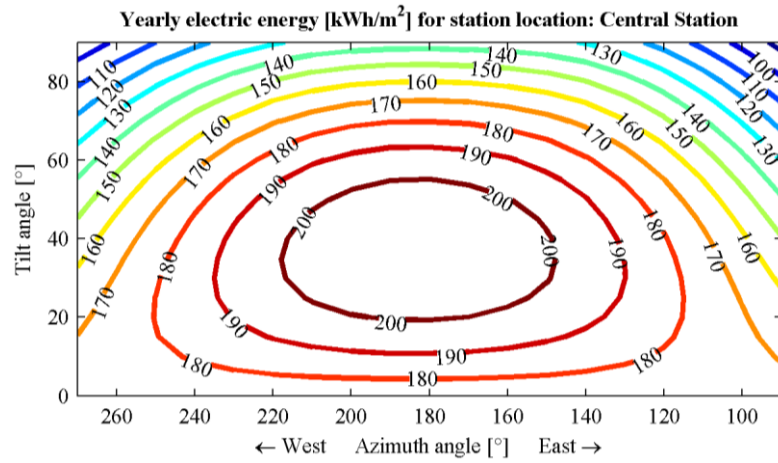


Figure A4-2. Contour plots of the yearly electric energy yield for the studied station locations depending on azimuth and tilt angle.





## Appendix 5

The following graphs show the effect of different solar panel areas on the share of time a grid-connected system do not take energy from the grid with different stationary battery sizes.

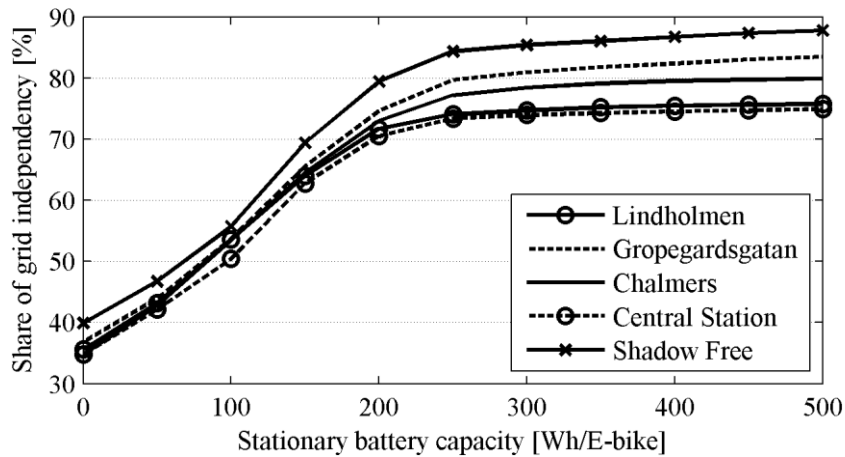


Figure A5-1. Solar panel area: 1.5 m<sup>2</sup> and 10.8 trips/(bike & day).

Share of the time there is no interaction with the grid depending on the size of the stationary battery.  
The rider profile used in all cases was the commuter.

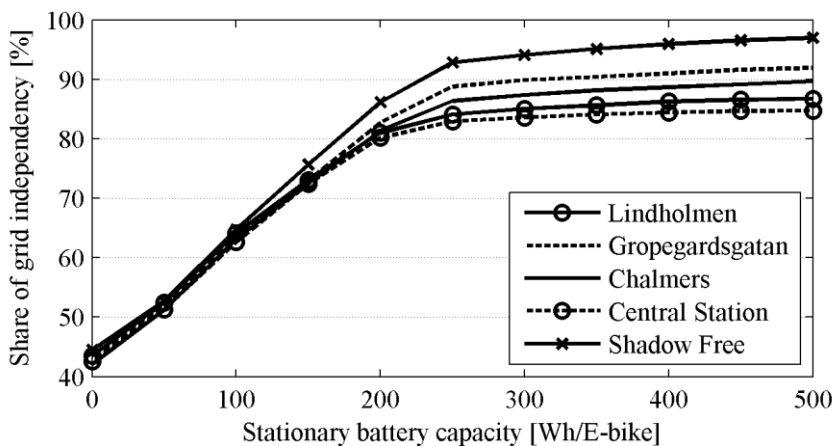


Figure A5-2. Solar panel area: 3 m<sup>2</sup> and 10.8 trips/(bike & day).

Share of the time there is no interaction with the grid depending on the size of the stationary battery.  
The rider profile used in all cases was the commuter.

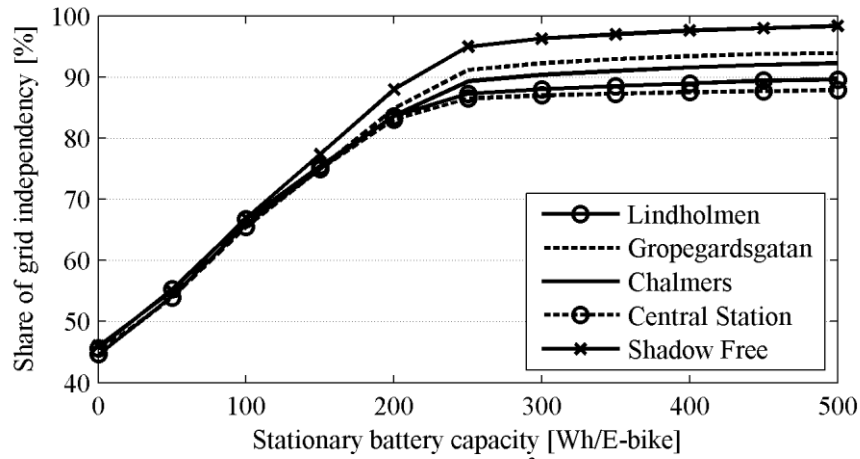


Figure A5-3. Solar panel area:  $3.8 \text{ m}^2$  and  $10.8/(\text{bike} \ \& \ \text{day})$ .

Share of the time there is no energy flow from the grid depending on the size of the stationary battery.  
The rider profile used in all cases was the commuter.

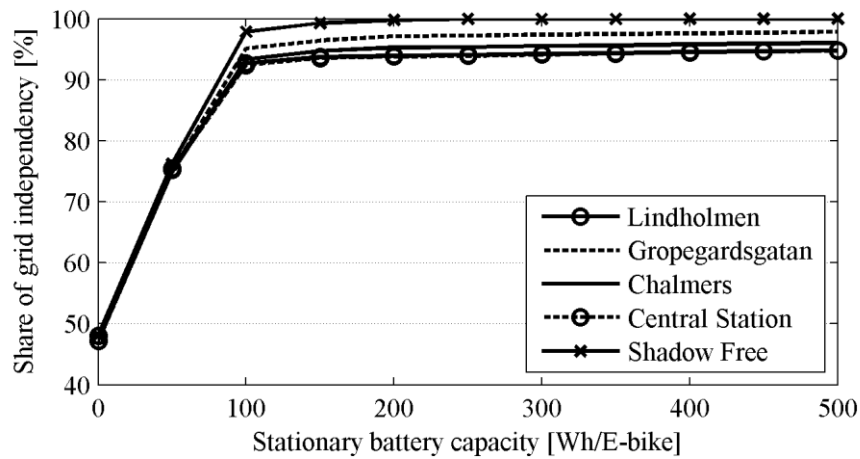


Figure A5-4. Solar panel area:  $2 \text{ m}^2$  and 4 trips/(bike & day).

Share of the time there is no energy flow from the grid depending on the size of the stationary battery.  
The rider profile used in all cases was the commuter.

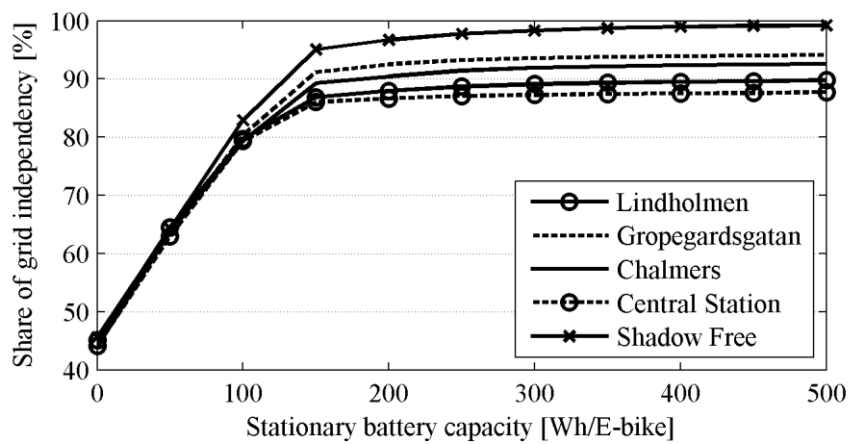


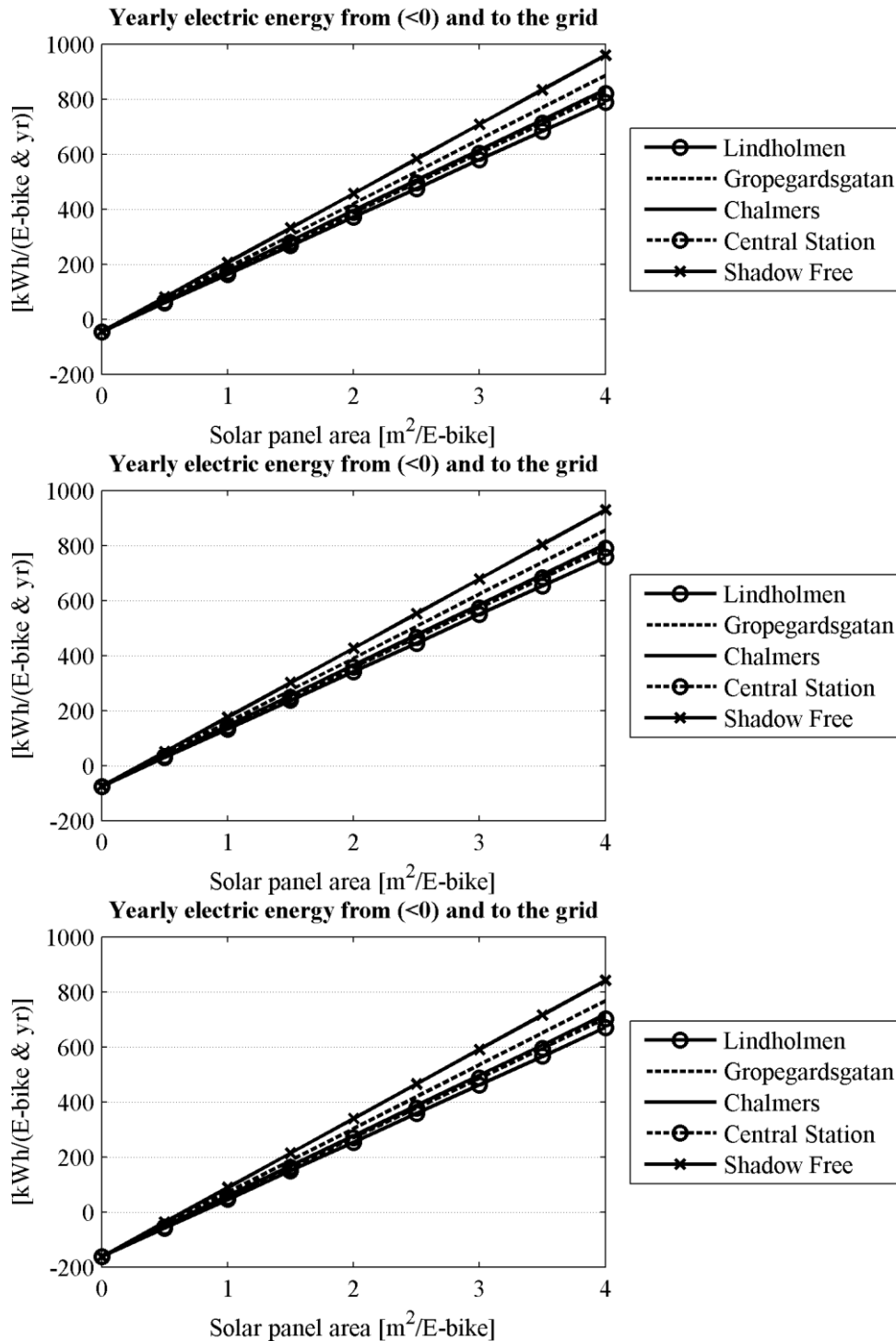
Figure A5-5. Solar panel area:  $2 \text{ m}^2$  and 3 trips/(hour and day).

Share of the time there is no energy flow from the grid depending on the size of the stationary battery.  
The rider profile used in all cases was the commuter.

## Appendix 6

Shown below is the yearly energy balance depending on solar panel area for three different trips uses, 3, 5 and 10.8 trips/(bike & day).

Figure A6-1. The yearly electric energy balance per E-bike depending on solar panel area.  
Use: 3, 5 and 10.8 trips/(bike & day) respectively, rider profile: commuter.



## Appendix 7

This appendix shows the hours of E-bike battery depletions per day for the studied period and an off-grid system. Using a buffer battery would reduce the peak depletions.

*Figure A7-1. 3 trips/(bike and day),  
First graph: 1 m<sup>2</sup> solar panel/bike. Second graph: 2 m<sup>2</sup> solar panel/bike.*

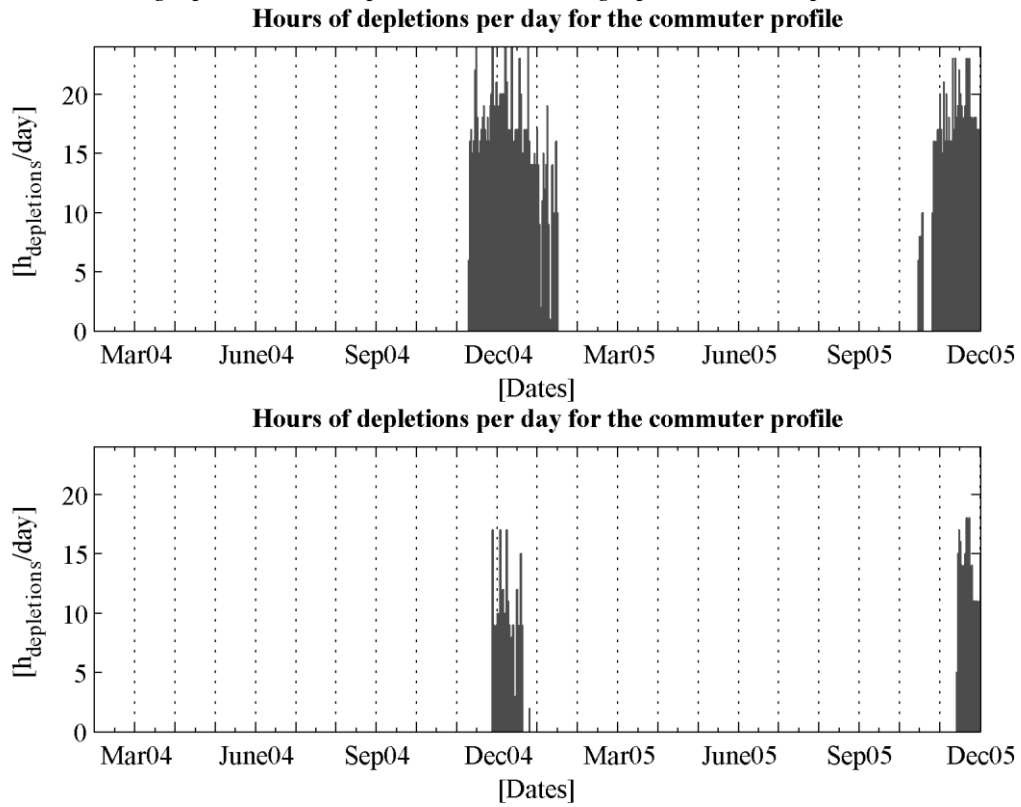


Figure A7-2. 5 trips/(bike and day),  
First graph: 1 m<sup>2</sup> solar panel/bike. Second graph: 2 m<sup>2</sup> solar panel/bike.  
**Hours of depletions per day for the commuter profile**

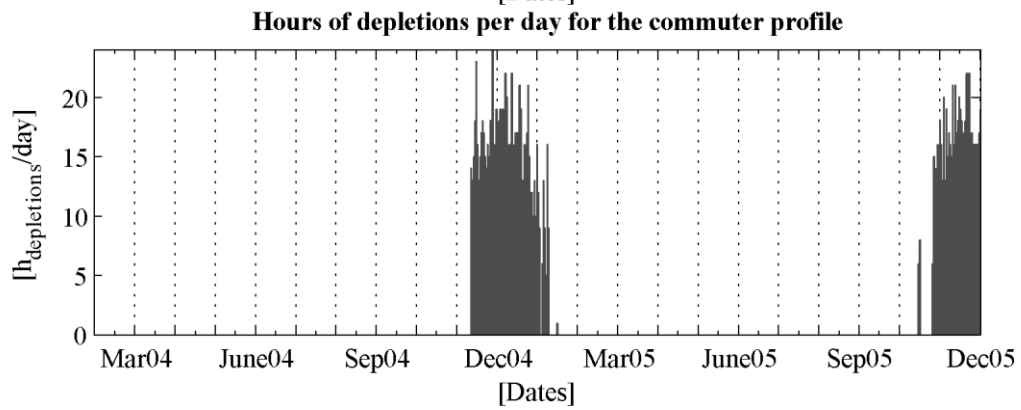
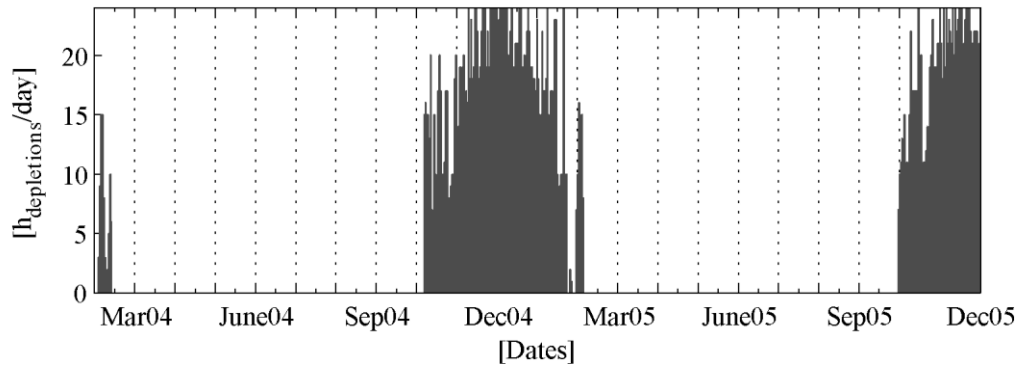


Figure A7-3. 10.8 trips/(bike and day),  
First graph: 1 m<sup>2</sup> solar panel/bike. Second graph: 2 m<sup>2</sup> solar panel/bike.

